INVESTIGATION OF *IN VITRO* LOADING AND RELEASE KINETICS OF HYDROXYAPATITE/CELLULOSE BIOCOMPOSITES

By

BENJAMIN MAWULI GANE

(10479794)

THIS THESIS IS SUBMITTED TO THE UNIVERSITY OF GHANA, LEGON IN PARTIAL FULFILMENT OF THE REQUIREMENT FOR THE AWARD OF MPHIL BIOMEDICAL ENGINEERING DEGREE

UNIVERSITY OF GHANA

COLLEGE OF BASIC AND APPLIED SCIENCES

DEPARTMENT OF BIOMEDICAL ENGINEERING

DECEMBER 2021

DECLARATION

I, Benjamin Mawuli Gane, do hereby declare that the work in this thesis titled "**Investigation of *in vitro* loading and release kinetics of hydroxyapatite/cellulose biocomposites**" was carried out and written by me under strict supervision according to the academic rules and regulations of University of Ghana and that this thesis has never been presented either in part or in whole for any degree in this University or elsewhere.

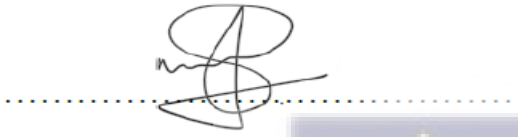

…20/12/2021…

Benjamin Mawuli Gane (10479794) Date

(Student)

This thesis has been submitted for examination with our approval as supervisors.

…… …20/12/2021…

Prof. Elvis K. Tiburu Date

(Principal Supervisor)

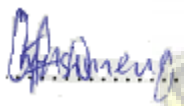

…… …20/12/2021…

Dr. Bernard Asimeng Date

(Co-Supervisor)

ABSTRACT

Cellulose nanocrystal (CNC) and hydroxyapatite (HAP) offer numerous advantages in drug delivery. A significant challenge encountered is the occurrence of burst release when these materials are used as drug carriers. This renders drugs ineffective when used at sites that require a sustained release. In this work, CNC and HAP composites were synthesized and used as drug carriers to investigate the release behavior of a model drug (curcumin). Two synthesis techniques were used where one material serves as the base material and the other as a modifier in varying concentrations. The formulated composites were characterized by Fourier-transform infrared spectroscopy (FTIR) and X-Ray powder Diffraction (XRD). The drug was loaded onto the composites for 22 hours. Composites with HAP as base material demonstrated successful loading of curcumin whereas composites with CNC as base material did not exhibit drug uptake. There were no significant differences ($p > 0.05$) in terms of drug uptake between the formulated composites and the control (HAP). The release properties of the composites were evaluated *in vitro* for 6 hours at acidic (pH ≈ 6.2) and basic (pH ≈ 7.4) conditions. The percentage drug release in acidic medium was found to be higher than basic medium. One-way ANOVA revealed that there was no difference in the means of the release data between the composites and the control group at acidic pH ($p > 0.05$). However, at basic condition, the release data of the composites and the control group showed significant differences ($p < 0.05$). Significant differences ($p < 0.01$) were observed for all composites across groups, indicating that changes in pH had a significant effect on the drug release. All composites and control at both pH (6.2 and 7.4) were best described by the Korsmeyer-Peppas model. Cell viability studies showed that modified composites inhibited cell growth at all time points during the drug release as compared to HAP only. This shows that the combination of HAP and CNC serves as a better drug delivery system than HAP only.

DEDICATION

I dedicate this thesis to the Almighty God, my parents and to everyone who played an important role in my life.

ACKNOWLEDGEMENTS

First and foremost, I thank the almighty God for His strength throughout my graduate study. My profound gratitude goes to my supervisors. Prof. Elvis K. Tiburu and Dr. Bernard Asimeng for their invaluable advice, continuous support, encouragement and constructive suggestions on this study. I gratefully recognize the help of Mr. Solomon Kingsley Katu for his assistance in keeping my progress on schedule and offering me the resources available in the laboratory for my research work. Special thanks to Dr. Martin Egblewogbe and Mr. Samuel Owusu-Atuah for their help in the X-Ray powder Diffraction (XRD) and Fourier-Transform Infrared spectroscopy (FTIR) characterizations respectively. I would also like to thank Mr. Edward Amenyaglo for his enormous help. I also thank Mr. Alex Atia, the Assistant Overseer at the Department of Biomedical Engineering.

Finally, I wish to thank my parents (Mr. Benjamin Seloame Gane and Mrs. Charlotte Agudu) and Ms. Benedicta Bubune Adatorvor for their prayers, support and encouragement throughout the entire study.

TABLE OF CONTENTS

DECLARATION ii

ABSTRACT iii

DEDICATION iv

ACKNOWLEDGEMENTS v

LIST OF TABLES x

LIST OF FIGURES xi

LIST OF ACRONYMS AND ABBREVIATIONS xii

CHAPTER ONE 1

1.0 Introduction 1

1.1 Background 1

1.2 Problem statement 6

1.3 Research question and hypothesis 6

1.3.1 Research questions 7

1.3.2 Hypothesis 7

1.4 Aim and objectives 8

1.5 Scope and limitations 8

1.5.1 Scope 8

1.5.2 Limitations 9

CHAPTER TWO 10

2.0 Literature review 10

2.1 Drug delivery 10

2.1.1 Drug delivery methods 12

2.1.2 Drug delivery systems 12

2.1.3 Requirements for drug delivery systems 14

2.2 Cellulose nanocrystals (CNCs) 16

2.2.1 Modification of CNC 19

2.3 Hydroxyapatite (HAP) 20

2.3.1 Modification of HAP 22

CHAPTER THREE 24

3.0 Materials and Experimental Techniques 24

3.1 Materials and chemicals 24

3.2 Experimental methods 24

3.2.1 Dissolution of CNC 24

3.2.2 Dissolution of HAP 25

3.2.3 Composite Formation 25

3.2.3.1 CNC as base material 25

3.2.3.2 HAP as base material. 26

3.2.4 Calibration Curve of Model Drug (Curcumin) 26

3.2.5 Drug Loading 26

3.2.6 *In vitro* drug release 28

3.3 Material Characterization Methods 28

3.3.1 Fourier-Transform Infrared spectroscopy (FTIR) 28

3.3.2 X-ray powder diffraction (XRD) 29

3.3.3 Ultraviolet-visible spectroscopy (UV-VIS) 29

3.4 Cell viability studies 31

3.4.1 Cell culture conditions 31

3.4.2 MTT assay 31

3.5 Data analysis 32

CHAPTER FOUR 34

4.0 Results and Discussion 34

4.1 Fourier-transform infrared spectroscopy (FTIR) 34

4.1.1 Composites with CNC as base material 34

4.1.2 Composite using HAP as base material. 36

4.2 X-Ray Diffraction (XRD) 38

4.2.1 Composites with CNC as base material 38

4.2.2 Composites with HAP as base material 40

4.3 Standard calibration curve of model drug (curcumin) 42

4.4 Drug loading 43

4.5 Drug release characteristics 46

4.6 *In vitro* drug release kinetics 50

4.6.1 Drug release in pH ≈ 6.2 50

4.6.2 Drug release in pH ≈ 7.4 51

4.7 Cell viability 55

CHAPTER FIVE 58

5.0 Summary 58

5.1 Conclusion 58

5.2 Recommendation 60

6.0 References 61

7.0 Appendices 79

LIST OF TABLES

Table 4.1: Crystallinity of samples in the range 20° – 25° 2θ 40

Table 4.2: Summary of crystallinity of samples 41

Table 4.3: Entrapment efficiency of composites with HAP as base material 45

Table 4.4: Percentage cumulative release of curcumin from composites 46

Table 4.5: R-squared values from fitted models 54

LIST OF FIGURES

Figure 2.1: Pharmacokinetic profiles of sustained release vs. conventional release of drugs. 11

Figure 2.2: Different types of carriers used for drug delivery 16

Figure 2.3: Chemical structure of CNC showing the rich hydroxyl groups 19

Figure 2.4: Chemical structure of hydroxyapatite. 22

Figure 3.1: CNC powder in solvent system 24

Figure 3.2: HAP powder in 5% glacial acetic acid 25

Figure 3.3: Agitation of composites in drug solution to ensure adsorption of drug 27

Figure 4.1: FTIR spectra of composites with CNC as base material 36

Figure 4.2: FTIR spectra of composites with HAP as base material. 37

Figure 4.3: XRD plot of composites with CNC as base material. 39

Figure 4.4: XRD plot of composites with HAP as base material. 41

Figure 4.5: Standard calibration curve of curcumin 42

Figure 4.6: Drug upload on CNC and composites with CNC as base material 44

Figure 4.7: Drug upload on HAP and composites with HAP as base material..... 45

Figure 4.8: Drug release profiles of samples in acidic medium (pH ≈ 6.2)..... 47

Figure 4.9: Drug release profiles of samples in neutral medium (pH ≈ 7.4) 48

Figure 4.10: Higuchi release profile of all samples 52

Figure 4.11: Korsmeyer-Peppas release profile of all samples..... 52

Figure 4.12: Cubic degree polynomial release profile of all samples..... 53

Figure 4.13: Cell viability of all composites and control using MTT assay. 55

Figure 4.14: Cell viability of 2.0 mg CNC/HAP composite using MTT assay. 57

Figure 4.15: Cell viability of HAP using MTT assay. 57

LIST OF ACRONYMS AND ABBREVIATIONS

ANOVA	One-way analysis of variance
CNC	Cellulose nanocrystal
CTAB	Cetyltrimethylammonium bromide
DDS	Drug delivery system
DMSO	Dimethyl sulfoxide
FTIR	Fourier Transform Infrared Spectroscopy
HAP	Hydroxyapatite
LiOH	Lithium hydroxide
MTT	3-(4, 5-dimethylthiazolyl-2)-2, 5-diphenyltetrazolium bromide
NaOH	Sodium hydroxide
NP	Nanoparticle
PVA	Poly (vinyl alcohol)
SDS	Sodium dodecyl sulfate
SEM	Scanning Electron Microscopy
UV	Ultraviolet
UV-Vis	Ultra-violet Visible spectroscopy
XRD	X-Ray powder Diffraction

CHAPTER ONE

1.0 Introduction

This chapter presents a standard synopsis of the project considering the project's background, research justification, problem statement, aim and objectives, research question and hypothesis, the scope and limitations.

1.1 Background

There has been an unprecedented growth in the field of nanotechnology research pertaining to drug delivery in the treatment of diseases. This is observed as researchers investigate various approaches for diagnosis and treatment for cancer. Nanotechnology is defined by the National Nanotechnology Initiative in the United States as the understanding and control of matter at nanoscale dimensions which is approximately 1 to 100 nanometers (Heath, 2015). Nanoparticles (NPs) are used as drug carriers as they can deliver active ingredients targeted to malignant cells or tissues without causing harm to surrounding healthy cells and tissues while producing a desired pharmacological effect. NPs that act as drug carriers should be biodegradable, should not trigger any immunological response, and be able to release the drug at the target site (Portioli et al., 2017). NPs provide major advantages over conventional delivery methods in terms of high stability, high specificity, high drug loading capacity, capability for controlled release of drug and the ability to transport both hydrophilic and hydrophobic molecules. Despite the numerous advantages of NPs as drug delivery systems, they still pose some challenges which include burst or rapid release at targeted sites that require a sustainable or prolonged release and goes a long way to affect therapeutic efficiency.

There is a growing demand for drug carriers that provide long-term drug release. Material composites are considered in order to make the development of these types of drug carriers easier.

However, the uniformity of these composite materials has an impact on drug release rates. According to Huang and Brazel's research, drug release is influenced by drug dispersion heterogeneity (Huang & Brazel, 2001). As a result of the heterogeneous dispersion of drugs introduced by the aggregation of composites, caution should be exercised during material processing for composite formation to be used as drug carriers.

Combining organic and inorganic materials results in enhancing their individual physical and chemical properties. These enhanced properties possess various characteristics (Sanchez, Julián, Belleville, & Popall, 2005) which are used in many applications particularly in biomedical fields. Biopolymers such as cellulose, chitosan, collagen and alginate among others are usually incorporated into nanocomposites due to their outstanding properties such as biocompatibility, biodegradability and availability. Cellulose has however received much attention with a number of applications ranging from paper, textile, and composite to pharmaceutical excipients for over the past years (Eyley & Thielemans, 2014).

Cellulose has been found to be readily available and the most sustainable biopolymer on earth (Moniri et al., 2017). Generally, cellulose has the same molecular formula $(C_6H_{10}O_5)n$, irrespective of its source. Various sources of cellulose are wood, plant fibers, bacteria and invertebrates among others. Plant cellulose, unlike bacterial cellulose, contains lignin, hemicelluloses, and pectin which compromises the purity of cellulose from plants. However plant cellulose are highly soluble than cellulose from bacterial source (Zhong, 2020). Chemically, cellulose is a linear polysaccharide made up of glucose monosaccharide units that link each other by β-1-4 glycosidic bond (Kenawy et al., 2020). Intermolecular hydrogen bonds bind hydroxyl groups and oxygen atoms to glucose in a rigid and stable ring structure. Comparatively such rigid intermolecular bonds to the glucose base is in multiples and highly stable in bacterial cellulose making it uneasy to dissolve (Lee,

Blaker, & Bismarck, 2009). These cellulose molecules exist as fibers (which are about 5-50 nm in diameter) held together by intramolecular hydrogen bonds and van der Waals interactions. Thus, cellulose is partially soluble in water and some solvents unlike alcohol. This is as a result of the strong intramolecular and intermolecular hydrogen bonding between the chains that make up cellulose (Lee et al., 2009). Such a limitation can be mitigated by doping cellulose with other polymers or inorganic materials such as HAP (hydroxyapatite) to break and limit inter and intramolecular hydrogen bonds. Depending on the type of application, cellulose is purified and separated into its nanocrystal components**.** To separate into nanocrystals, cellulose is treated with an acid which catalyzes the amorphous regions, thereby leaving the crystalline regions only (Shankaran, 2018). The purification methods include treatment with sodium hydroxide (NaOH) or sodium dodecyl sulfate (SDS) (Banerjee, Saraswatula, Williams, & Brettmann, 2020). It is reported in literature that a synthesized poly(vinyl alcohol) PVA/cellulose composites exhibited a highly proven mechanical and thermal properties and also a high flexibility as compared to the pure cellulose only (Dai, Wang, Samanipour, Koo, & Kim, 2016). In another paper, Poly (ethylene oxide)/cellulose nanofiber biocomposites were formulated by aqueous solution method. The results showed that the modified biocomposites exhibited enhanced mechanical properties. These works show that blended polymer biocomposites showed improved properties which can be used for many biomedical applications (Safdari, Carreau, Heuzey, Kamal, & Sain, 2017).

Cellulose's biocompatibility *in vitro* and *in vivo* has been proven by several studies. Research has shown that plant cellulose-derived scaffolds had a promising potential when subcutaneously implanted in wild immunocompetent mice. The scaffolds supported the production of natural extracellular matrix and promoted vascularization (Modulevsky, Cuerrier, & Pelling, 2016). Literature also reported the *in vivo* and *in vitro* evaluations of plant-derived cellulose hydrogels

enriched with *Larrea tridentata* in a rat model. It showed no negative effect on their biocompatibility properties (Tovar-Carrillo et al., 2020). A study reported a fabrication method of plant-derived scaffolds that support cell attachment and invasion both *in vitro* and *in vivo*. Their fabrication method is reported to improve cell attachment and the scaffold remains highly biocompatible and maintains *in vivo* vascularization properties (Hickey, Modulevsky, Cuerrier, & Pelling, 2018). These studies affirm the biocompatibility of plant cellulose and the reason why it is useful in diverse range of applications especially biological or medical applications. The use of cellulose nanocrystal (CNC) as a drug carrier is becoming more popular. Most drugs released from this polymer, however, are released rapidly, which could be due to ion exchange between ions on the CNC surface and ions present in the release medium (Jackson et al., 2011). This affects the therapeutic efficiency of the drug at sites that require sustained released of drug. CNC is also being studied as a composite material due to its large surface area, high aspect ratio, and tremendous stiffness and strength (Jackson et al., 2011). Combining CNC and a polymer or inorganic material as a composite material may result in a prolonged or sustained release.

The use of inorganic nanoparticles has aroused interest among scientists. The high surface energy of inorganic nanoparticles makes them thermodynamically unstable (Huang, Li, Liu, He, & Tan, 2015). However, from experiments, during the production and treatment of these inorganic nanoparticles, agglomeration, which is a challenge, occurs leading to the aggregation of the individual materials involved. This comes about as a result of the attraction of the particles through chemical bonding as the nanoparticles are being formed in surfactant-free chemical reactions. This affects their properties and applications (Li & Kaner, 2006). The study further reported that this limitation is solvable by causing the nanoparticles that are formed to be absorbed onto a supporting material, examples being an inorganic material or a polymer. Research works are geared towards

using these inorganic nanoparticles in the biomedical field. A typical example is the use of hydroxyapatite (HAP) as drug carriers because it possesses no, or minimum toxicity and it is one of the excellent biocompatible materials since it is found in the human teeth and bone. Despite the numerous advantages of HAP, it has also been proven that drugs released from HAP is very fast due to weak interaction between the drugs and HAP. This weak interaction is due to electrostatic interactions between the ions on HAP and the drug (Mizushima et al., 2006). This challenge can be reduced by combining HAP nanoparticles with a polymer which will result in a prolonged release of the drug. From literature, polymer/HAP composites are used to achieve sustained release of drug molecules, growth factors and as scaffolds for cell growth (Wei & Ma, 2004).

Typically, in the synthesis of inorganic nanoparticles, large aggregates are formed instead of well dispersed nanoparticles due to the presence of high surface energy. This aggregation is caused by hydrogen bonding and van der Waal's forces (Laaksonen, Ahonen, Johans, & Kontturi, 2006). To mitigate this problem, the surfaces are mostly protected. Stabilizers are added during the aqueous synthesis of inorganic nanoparticles to help control the nucleation, growth rate, and particle shape of the nanoparticles. The stabilizers with metal affinity groups bind to the inorganic surface and thus induce repulsive forces which help to stabilize the inorganic particles. When the stabilizers degrade or undergo oxidation, the stabilization of the inorganic nanoparticles is compromised. Also, conditions such as pH change and the charge present on the inorganic nanoparticle surface is affected resulting in the initiation of nanoparticle aggregation (Sperling & Parak, 2010).

Another approach in resolving the problem of aggregation of the particles is by depositing inorganic nanoparticles onto a material with high surface area. Literature has reported that carboxylic or sulphonic acid groups offer longer stability for inorganic nanoparticles (Sperling & Parak, 2010). The above approaches will prevent aggregation and make the formulated composites

suitable to be used as a drug carrier for sustained release of drugs. Research scientists have gained interest in the use of biomaterials from plants for various biomedical applications, for example the use of CNC as a substrate to promote the growth of HAP crystals.

In this work, CNC and HAP were functionalized, a model drug (curcumin) was loaded onto the resulting composites and released at pre-determined times. The functionalized composites were characterized by Fourier-Transform Infrared spectroscopy (FTIR) and X-Ray powder Diffraction (XRD), and the release studies were done by Ultra-violet Visible spectroscopy (UV-Vis). The release study and kinetics of the composites were examined by using existing kinetic models.

1.2 Problem statement

Cellulose nanocrystal and hydroxyapatite when used as drug carriers, exhibit burst release of the drug (Mizushima et al., 2006; Jackson et al., 2011). This affects therapeutic efficiency when used at targeted sites that require a sustained release of the drug. This, therefore, increases the ineffectiveness of the drug. Despite the numerous advantages of polymers and inorganic materials as drug carriers, they still pose some challenges which include sustained and safe delivery of drug to cells for improved efficacy. Most of these materials have not been able to completely deliver sustainably on the promise of targeted diseased sites (Pasut, 2019).

1.3 Research question and hypothesis

The purpose of this research is to provide answers to questions raised by literature and to lay the framework for adopting or rejecting the hypothesis indicated below.

1.3.1 Research questions

1. Can CNC (as a base material) be modified with HAP?
2. Can HAP (as a base material) be modified with CNC?
3. Can the modified composites be loaded with the model drug (curcumin)?
4. Does the interaction between the composites enhance the release rate of the drug?
5. What is the effect of pH on the rate of release of the drug (curcumin)?
6. How do the modified composites affect the delivery of curcumin to MDA-MB-231 cells?

1.3.2 Hypothesis

Hydroxyapatite (HAP) and cellulose nanocrystals (CNC) possess complementary properties and are compatible which will ensure effective interfacial bonding between them and result in composites with improved properties and functionalities. The composites formed from HAP and CNC will be capable of loading the model drug curcumin and exhibit sustained release properties resulting in improved drug delivery characteristics. The pH of the surrounding environment influences the release rate of drugs from modified composites leading to different rates of drug release depending on variations in pH. It is therefore predicted that the drug release profile will exhibit a pH-dependent behavior with a more pronounced effect observed at extreme pH levels. It is also anticipated that the modified composites will exhibit controlled drug release, thereby effectively reducing cell viability.

1.4 Aim and objectives

The aim of this work is to synthesize hydroxyapatite/cellulose biocomposites for sustained release of drug to improve therapeutic efficiency. To achieve the overall aim of this work, the following objectives will be followed:

1. Synthesize and characterize HAP/CNC composites using HAP and CNC as base materials.
2. Assess drug upload and release kinetics in the HAP/CNC composites.
3. Examine the drug release kinetics of the HAP/CNC composites in different pH.
4. Assess the impact of loaded composites on drug delivery to MDA-MB-231 cells.

1.5 Scope and limitations

1.5.1 Scope

This work centers primarily on using HAP to modify CNC and to use CNC which is a polymer as a dopant during the synthesis of HAP as a base material. The model drug will be loaded on the resulting composites and study the release kinetics at different pH (6.2 and 7.4). The thesis will consist of 5 chapters. Chapter one will be the introduction, which gives a background of this research, the objectives and the relevance of the work. Chapter two will talk about literature review, which surveys scholarly articles, books and other sources relevant to this research. Chapter three will outline the materials and techniques used. Chapter 4 will cover the results and discussions of the findings and chapter five, which is the last chapter, will be the conclusion of the work with some recommendations.

1.5.2 Limitations

The following studies were not covered in this work:

i. Zeta potential of synthesized composites.

ii. Scanning Electron Microscopy (SEM) of composites.

CHAPTER TWO

2.0 Literature review

This chapter reviews the underlining theoretical concepts used in this work. It focuses on drug delivery systems, synthesis of cellulose nanocrystals and hydroxyapatite, drug release studies from synthesized composites in literature.

2.1 Drug delivery

Drug Delivery is a fast-evolving multidisciplinary field within the health sciences. Drug delivery is a broad field which describes the development of novel carrier systems for safe and effective delivery of therapeutic agents to their site of action to achieve therapeutic effect (Tiwari et al., 2012). Pharmacodynamics and pharmacokinetics are essential for drug delivery. Pharmacodynamics describes the physiologic and biochemical effects of the drug on the body (Rimmington, 2020). Pharmacokinetics refers to the time course of the concentration of a drug in the body, from absorption, bioavailability, distribution, metabolism through to excretion (Thürmann, 2020). For a disease to be properly managed, pharmacokinetic profiles of therapeutic drugs must be consistent. This is contingent on the patient's continued compliance in taking the medication as prescribed. Patients on prolonged release therapies have been shown in the literature to have lower rates of relapse due to constant dosing of the medicine (Senior, Radomsky, & Group, 2000). This enables the achievement of a consistent and stable pharmacodynamics profile. Conventional method of drug delivery is effective when a quick response of the drug is required. However, drugs with narrow therapeutic window and low solubility are ineffective when delivered by the conventional method.

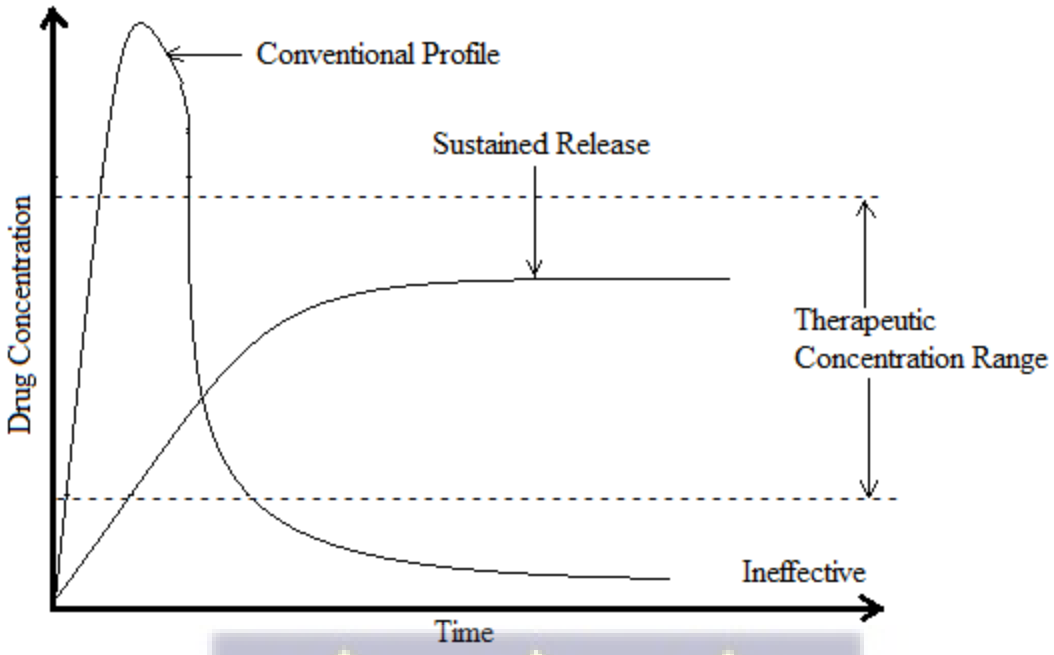

Figure 2.1: Pharmacokinetic profiles of sustained release vs. conventional release of drugs. Adapted from "Modeling of controlled-release drug delivery from autocatalytically degrading polymer microspheres" by A. F. Versypt (2015)

In figure 2.1, sustained release is achieved when a drug concentration increases steadily and plateaus in the therapeutic range in the blood plasma of a specific target and releases the drug for an extended period and that is where maximum therapeutic efficiency is reached. When the drug concentration goes above the therapeutic range, it is considered toxic and when the concentration goes below the therapeutic range, it is rendered ineffective. The first controlled release formulation was approved in the 1950s (Lee & Li, 2010). Since then, there has been a steady increase in the development of new carriers for drug delivery as compared to development of new drugs (Park, 2014). One of the major factors for this shift is due to the high cost and time involved in developing new drugs. A review in 2013 found that the cost involved in developing a drug carrier was 10% of the cost of developing a new drug (He et al., 2013). As such research scientists prefer to develop drug carriers to increase the effectiveness of drug targeting and delivery other than go through the

long process of drug discovery, clinical testing, and drug development through to regulatory approval.

2.1.1 Drug delivery methods

Drugs are administered by swallowing, absorption, inhalation, intravenous injection, or through the skin to create a systemic pharmacological effect. The oral route which is the common route experiences the following problems: low bioavailability, poor absorption of protein and this results in low permeability of drugs (Gopinath & Wilson, 2020). For pulmonary delivery as a route for systemic administration, inhalation is used. Intravenous infusion is often used to deliver sedatives, analgesics, chemotherapy agents, anesthetics and other fluid to patients (Ferrari, Sponchioni, Morbidelli, & Moscatelli, 2018). For transdermal route of drug delivery, the skin acts as a barrier allowing molecules with appropriate physiochemical properties to penetrate the skin (Alkilani, McCrudden, & Donnelly, 2015). Some advantages of delivery of drugs through the skin are less frequent dosing, large area for absorption and noninvasiveness among others (Saravanakumar, Swapna, Nagaveni, Vani, & Pujitha, 2015).

2.1.2 Drug delivery systems

Drug delivery systems (DDSs) are pharmaceutical formulations or engineered devices that aid in the targeted delivery and/or controlled release of pharmaceutical compounds in the body and improves its efficacy and safety by regulating the rate, timing, and location of medication release in the body (Jain, 2020). DDSs release active pharmaceutical compounds when administered. When these compounds are encapsulated within a protective structure, potential disruptions of the active compounds are reduced (Wang et al., 2021). Aside the increment in bioavailability of the pharmaceutical compound, undesirable side effects resulting from systemic distribution and frequent dosing are reduced (Kok-Yong & Lawrence, 2015). The bioactive molecules reach the

site of action as they pass through many biological barriers. Research has revealed that these barriers play different roles in the transport of drugs in the circulatory systems and through cells and tissues (Yang et al., 2017). Research scientists have capitalized on the roles of these biological barriers to develop new modes of drug delivery. Current novel DDSs trigger the release of the drug only at the target site with sustained or controlled release. Others deliver based on stimuli such as light, and temperature among others. One important advantages offered by delivery systems is the controlled drug release in a time dependent manner through passive and active targeting (Kumar & Gupta, 2012). Passive targeting works based on the pathophysiological features of tumor vessels which allow DDS to accumulate in the tumor at much higher concentrations than in normal tissues since tumor vessels become more permeable than healthy state and the compromise of the lymphatic drainage in tumors also enhances the retention of theses delivery systems in tumors (Attia, Anton, Wallyn, Omran, & Vandamme, 2019). This type of targeting depends on the size and circulation time of the delivery system. Active targeting relies on the ligand-receptor binding, which improves the accumulation of DDS to target sites (Yoo, Park, Yi, Lee, & Koo, 2019). This facilitates the uptake of DDS by the tumor cells. DDS could be activated by a trigger that is peculiar to the target site, such as a pH responsive material. Example, most parts of the body have a consistent neutral pH. Some other parts may become more acidic than others, especially tumor environments. DDSs can however use the change in pH to trigger the release of the drug. Another mechanism that can be used to trigger drug release is the redox potential (Mollazadeh, Mackiewicz, & Yazdimamaghani, 2021). Tumors change the redox potential in their environment. Based on this, a payload of drug can be released based on a change in redox potential in the tumors.

2.1.3 Requirements for drug delivery systems

Ideal Drug Delivery Systems ensure that drug is released at the targeted site of action in accordance with the need of patient for an intended duration. The concentration of the drug at the targeted site should be between minimal effective concentration and minimal toxic concentration (Hedaya, 2012). The DDSs must also regulate the rate of release of the drug in a controlled manner. Increase in patient compliance and reduction in frequency of drug dosing can be achieved when the drug fluctuation is reduced in the plasma level while extending its duration of action. The materials used for DDSs should not trigger any adverse response, the matrix material and its degraded products should be biocompatible, the mechanical properties of the material should be able to provide prolonged protection of the therapeutic cargo thus ensuring chemical stability of the drug before it gets to the target site (Parhiz et al., 2018). The surface of the DDS should be functionally modified for cell-specific moieties. There should also be a triggerable or controlled drug release. The stability of the product and delivery should be maintained under various physiological variables. They should be easy to administer to patients and ultimately, they should be safe and reliable.

Figure 2.2 illustrates various examples of DDSs that have been developed over the years, such as liposomes, micelles, polymeric particles, hydrogels, dendrimers, inorganic particles, quantum dots, and nanospheres. Liposomes are made up of one or more concentric phospholipid bilayers (Haisheng He et al., 2019). Polar drugs are loaded in its core because of its polar nature. They can entrap both amphiphilic and lipophilic compounds depending on the compounds' affinity towards the phospholipids. In literature, Ketoprofen drug was encapsulated in pharmacosomes and showed an improved dissolution of 93.3% as compared to free ketoprofen which showed 49.77% dissolution (Amandeep Kaur, 2013).

Dendrimers are highly branched and monodispersed with symmetrical structure. They have a central core, branching units and terminal functional groups (Dias et al., 2020). Ligands are attached to the terminal ends of dendrimers to enhance drug targeting. The dendrimers are functionalized by polyethylene glycol chains to keep them stable and protect them from Mononuclear Phagocyte System. It was observed from research that the solubility of aceclofenac, a nonsteroidal anti-inflammatory drug, was improved by using G0 PAMAM dendrimers. The study showed that the enhancement of aceclofenac was dependent on the concentration of the dendrimer (Patel, Basu, Dharamsi, Garala, & Raval, 2011).

Polymers used for drug delivery can be natural or synthetic. Polymeric system formulations can deliver drugs sustainably for a longer time duration based on the properties of the polymer used in the formulation. Polymers can be tuned to change its properties depending on its application (Sharma, Aiswarya, Mirza, & Saha, 2020). This makes research scientists gain interest in the use of polymers for drug delivery applications. Drug release from polymers are affected by the environment of the release media, diffusion from the polymer and the chemical nature of the delivery system. Wilson et al., (2010) developed tacrine loaded chitosan nanoparticles and coated with polysorbate 80 for anti-Alzheimer therapy. The synthesized particles showed improved drug-loading capacity and sustained release of drug.

Inorganic materials such as silica, graphene oxide, and hydroxyapatite and gold nanoparticles have been exploited for use in delivery of drugs. The nano-carriers which serve as skeletons in these systems are able to load and release drugs without compromising its framework in the blood (Zhaoqing Shi et al., 2020). They are biocompatible and possess good pharmacological properties. Lei et al., (2019) developed a drug delivery system by coating polydopamine on the surface of

mesoporous silica nanoparticles. The resulting carrier could respond to high glutathione or low pH to release drug. The diagram below shows some types of DDSs commonly used.

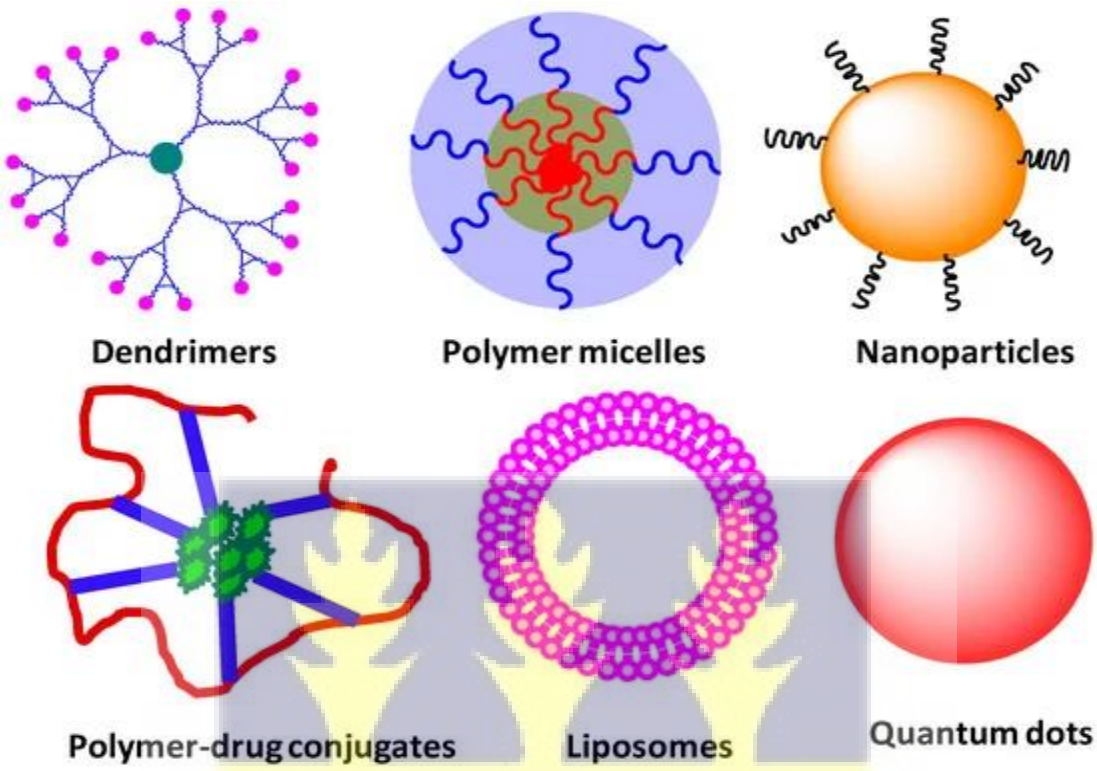

Figure 2.2: Different types of carriers used for drug delivery. From "Designing dendrimer and miktoarm polymer based multi-tasking nanocarriers for efficient medical therapy" by A. Sharma, & A. Kakkar. (2015). Molecules, Vol. 20, pp. 16987–17015.

2.2 Cellulose nanocrystals (CNCs)

Cellulose consists of crystalline and amorphous regions. Acid treatment of cellulose, irrespective of the source, hydrolyses the glycosidic bonds. This is in conjunction with the hydrolysis of the amorphous regions of cellulose. This is because the acid can permeate and catalyze the amorphous regions. The resulting crystalline units are referred to as CNCs. The size of the resulting nanocrystals depends on the source of the cellulose. Example CNCs from cotton are 70 – 300 nm (Elazzouzi-Hafraoui et al., 2008), from bacteria is 100 – 1700 nm (George & Siddaramaiah, 2012),

from wood; 100 – 300 nm (Beck-Candanedo, Roman, & Gray, 2005) in length. Hydrolysis using sulfuric acid results in the formation of sulfate esters on the surface of the nanocrystal. The hydroxyl groups of CNC as shown in figure 2.3, react partially with the acid to the formation of charged sulfate ester groups on its surface. This provides good dispersibility in aqueous suspension. The concentration of sulfuric acid and the duration of hydrolysis affect the number of sulfate groups present on the nanocrystal (Wang, Zhao, & Zhu, 2014). However, if CNC with no sulfate groups on the surface are required, then hydrobromic or hydrochloric acid is used in the hydrolysis (Montanari, Roumani, Heux, & Vignon, 2005). CNCs are rod-like in shape and have high aspect ratio (Habibi, Lucia, & Rojas, 2010), large surface area (Lam, Male, Chong, Leung, & Luong, 2012), high mechanical strength (Moon, Martini, Nairn, Simonsen, & Youngblood, 2011), high stiffness (Lam et al., 2012) and hydrophilic in nature (Farnia, Fan, Dory, & Zhao, 2019). The negatively charged surface of the CNC, along with its large surface area, enables the binding of high levels of drugs to its surface and the release of drugs by ion exchange processes in a regulated manner (Jain, Sahu, Mohan, & Jain, 2016). CNC can be distributed in polymer matrices of the same charge and bind with others of opposite charge. This results in a drug delivery system that releases drugs at a controllable rate. Research has shown the excellent sustained release of pilocarpine hydrochloride from poloxamer modified CNC up to more than twenty hours (Åhlén, Tummala, & Mihranyan, 2018). Abo-Elseoud et al., (2018) developed a contact lens platform for ocular drug delivery by incorporating *in situ* gelled nanoparticles and CNC in PVA lenses. The drug release was prolonged over 28 hours and the developed system exhibited a greater potential for extended drug release.

A study reported a burst drug release, followed by a slow and sustained release at 37°C when poly (N-isopropylacrylamide) reinforced with CNC was loaded with drug. The results showed that the

modified CNC has a good potential for being used as in ophthalmic drug delivery system and injectable hydrogels for wound dressing (Zubik, Singhsa, Wang, Manuspiya, & Narain, 2017).

There is the tendency of CNC aggregating when used in the preparation of nanocomposites though CNCs are well-dispersed in aqueous media. This arises due to lack of compatibility with the polymer which comes from the numerous surface hydroxyl groups as a result of the presence of strong hydrogen bonding (Wohlhauser et al., 2018). This challenge can be overcome by the introduction of an interaction between the polymer and CNCs. Preparation of CNC-polymer nanocomposites with covalent bonding between the polymer and CNC is one way to overcome the problem of aggregation (Meesorn, Shirole, Vanhecke, De Espinosa, & Weder, 2017). The direct attachment of polymer chains onto the surface of CNC creates the covalent bond. The binding of polymer chains to the CNC surface can be facilitated by the reactive functionality of the polymer chain (Kang, Liu, & Huang, 2015). The reacting polymer chains have larger groups and so have a significant steric hindrance to access the reaction site on CNC because of the presence of attached polymer chains (Chakrabarty & Teramoto, 2018). Another way aggregation can be prevented is by growing the polymer chains on CNC's surface. This is done by attaching species that initiate polymerization on the surface of CNC. Polymerization on the surface is highly probable in the presence of monomers and this will produce a high grafting density (Wu et al., 2015). The grafting process of other polymers through reactive hydroxyl groups on the surface of CNC yields low graft ratios. Researchers have gained interest in the functionalization of CNC with inorganic nanoparticles since the high surface area of CNC enhances nanocomposite formation between CNC and inorganic particles. Functionalization of CNC promotes the sustained release of drug since there will be a good dispersion of the drug in the absence of aggregation.

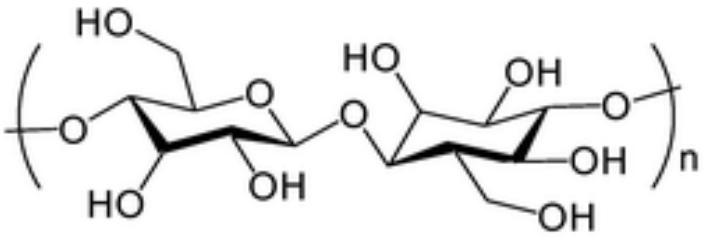

Figure 2.3: Chemical structure of CNC showing the rich hydroxyl groups. From "In situ nano-assembly of bacterial cellulose-polyaniline composites" by Z. Shi et al., (2012). RSC Advances, 2(3), 1040–1046.

2.2.1 Modification of CNC

Features such as biocompatibility, biodegradability and surface charge, among others have an effect on how drugs are released and delivered (Jackson et al., 2011). CNC is a good drug carrier for hydrophilic drugs due to its negative surface charge (Hare et al., 2017). The surface of CNC, which is rich in hydroxyl groups, may be modified with various chemical substances to other functional groups. Even though CNC does not carry hydrophobic drugs, the surface modification can enhance the loading and release of hydrophobic drugs like curcumin (Roman, Dong, Hirani, & Lee, 2009). Surface modification of CNC can also be employed to introduce new electrostatic properties (Kargarzadeh et al., 2018). This may also aid in drug delivery purposes and other applications. Some surface modification methods include cationization, sulfonation, oxidation, and silylation (Jorfi & Foster, 2015; Lam et al., 2012). Cationization has to do with the treatment of surface of a material with cations. This reduces the hydroxyl groups present on the surface of CNC. Oxidation introduces carboxylate groups onto the CNC surface which leads to better dispersion in aqueous phase. The reaction changes the C6 primary hydroxyl groups to carboxylate groups. Silylation refers to the introduction of a substituted silyl group to CNC typically through reactions with organosilane compounds. Sulfonation is the process of introducing sulfonic acid in

an organic compound. This replaces the hydrogen atoms present on CNC surface with sulfonic acid making the resulting compound more water-soluble. Another approach to modifying CNC involves the use of surfactant to coat their surface (Brinchi, Cotana, Fortunati, & Kenny, 2013). In a related study, the negative charge of CNC was successfully modified using a cationic surfactant called Cetyltrimethylammonium bromide (CTAB), resulting in CNC acquiring hydrophobic properties allowing for efficient loading of hydrophobic drugs within the CTAB domains. Notably, it was observed that the release of hydrophobic drugs from the modified CNC exhibited a slower rate compared to unmodified CNC (Brinchi, Cotana, Fortunati, & Kenny, 2013). These modifications enhance the surface hydrophobicity of CNC and facilitates the binding of hydrophobic drugs, leading to a sustained release profile for non-steroidal anti-inflammatory drugs (Gupta & Raghav, 2020) and curcumin (Raghav et al., 2020) among others. Similarly, another study reported the effect of natural surfactant saponin, on the modification of cellulose and starch nanoparticles through hydrophobic drug loading and release (Putro, Ismadji, Gunarto, Soetaredjo, & Ju, 2019).

2.3 Hydroxyapatite (HAP)

HAP with chemical formula $Ca_{10}(PO_4)_6(OH)_2$ is a bioceramic that is similar to the constituent of bones and teeth. It belongs to the calcium phosphates family. HAP has gained interest in science because of its exceptional characteristics; bioactivity and excellent biocompatibility (Mohd Pu'ad, Koshy, Abdullah, Idris, & Lee, 2019), absence of immune response (Ghiasi, Sefidbakht, & Rezaei, 2019), affinity to biopolymers (Setiawan, Widiyastuti, Winardi, & Nugroho, 2017) osteoinductivity and osteoconductivity (Yokota et al., 2018). HAP has good adsorptive properties due to the presence of its ion composition (Asimeng et al., 2019). HAP's thermodynamic stability in biological environment and adsorptive properties make it one of the best options for drug

delivery to cancer cells. HAP has a hexagonal structure (Luque et al., 2017) with high amount of hydroxyl on the surface and polar charge. This property makes it able to attract peptides and DNA (Sadat-Shojai, Khorasani, Dinpanah-Khoshdargi, & Jamshidi, 2013) and as such a good candidate for drug delivery systems for the controlled release of drugs (Andrés et al., 2018). However, the surface of pure HAP makes it lack biofunctionality which is a problem in drug delivery and this effect could be combated by adding a polymer to HAP to reduce leakage hence enhancing its biofunctionality. Research has reported that drugs loaded onto HAP are released very fast at the initial stage due to the weak force of interaction between drugs loaded and HAP particles (Zhu et al., 2015). Amidst the performance advantages of HAP, it has low strength and toughness, low fatigue resistance in biological environment. These disadvantages make it difficult for HAP to be used for medical and biological application. This problem can be alleviated by changing preparation methods of HAP and adding other materials like polymers to enhance its properties. Studies have reported the use of natural polymers such as chitosan, collagen, alginate, gelatin and starch to modify HAP which resulted in improved properties (Chen, Shi, Luo, & Ma, 2019).

Literature reported that HAP/chitosan composite showed an improved mechanical strength and biocompatibility. HAP nanoparticles were synthesized with polymers (polyvinyl alcohol and sodium alginate) and loaded with amoxicillin. Amoxicillin was observed to be released at a sustained rate for 30 days. The sustained release was achieved by coating HAP with polymers in a layer-by-later method (Prasanna & Venkatasubbu, 2018). Literature has reported enhancement in the antibacterial activity against *Staphylococcus aureus* through the introduction of silver-doped hydroxyapatite (Riaz et al., 2018).

Due to the chemical makeup and orientation of HAP crystals, they have two binding sites: C-sites (Ca^{2+}) and P-sites (PO_4^-) as shown in figure 2.4. In aqueous media, the C-sites are positively

charged and release OH^- ions from the surface of the crystal. Ca^{2+} ions interact with the negatively charged proteins after release of OH^- ions. The P-sites are negatively charged and thus interact with positively charged proteins (Haider, Haider, Han, & Kang, 2017). Literature confirmed that $–COO^-$ ions from leucine-rich amelogenin protein interacted with the surface of the HAP (Chen, Wang, Shen, Pan, & Wu, 2007). This confirms the presence of the C-sites on the surface of HAP. There are no side effects recorded for using HAP as drug carrier, there is enhanced bioavailability and efficacy. However, drawbacks still exist such as low mechanical strength and rapid release of the loaded drug.

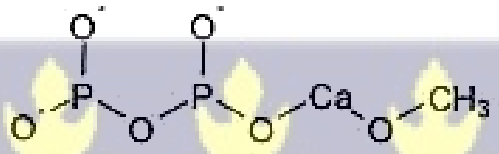

Figure 2.4: Chemical structure of hydroxyapatite. From "Direct crystal formation from micronized bone and lactic acid: The writing on the wall for calcium-containing crystal pathogenesis in osteoarthritis" by A.A. Bulysheva, N. Sori, & M. P. Francis, (2018). PLoS ONE, 13(11).

2.3.1 Modification of HAP

The surface of HAP is modified through ions adsorption, reprecipitation, encapsulation and surface reactions. The majority of surface ion exchange occurs due to hydroxyapatite's high specific surface area and the presence of a metastable hydrated layer on the surface containing loosely bound ions (Cazalbou et al., 2005). This is evident in the literature because apatites have metal ion sorption and exchange behavior to remove heavy metal ions from water or soils (Smičiklas, Onjia, Marković, & Raičević, 2005; Sugiyama et al., 2003). Reprecipitation is the process of dissolving a precipitate and precipitating it again. This ensures that metal ions are continuously distributed to the surface layer (Skwarek & Janusz, 2019).

Surface reaction of hydroxyapatite involves the reaction between ions present at the surface. An example of such a reaction is the adsorption of fluoride ions onto hydroxyapatite in aqueous solution. Calcium and phosphate ions together with fluoride ions were in solution and reacted. Fluoride was adsorbed to $H_2PO^-_4$ ions and favored the formation of brushite. As the amount of calcium was increased in the solution, calcium reacted with fluoride to form CaF_2 and was precipitated. Phosphate ions present favored the formation of fluorinated apatite (Gasser, Haikel, Voegel, & Gramain, 1994).

CHAPTER THREE

3.0 Materials and Experimental Techniques

This chapter explains the experimental approach used in this research work. The materials and chemicals used, synthesis of CNC/HAP composites, drug loading, release studies, characterization techniques have been described in this chapter.

3.1 Materials and chemicals

All reagents used for this work needed no further purification and were of analytical grade. Curcumin (99% purity), Cellulose Nanocrystals, Hydroxyapatite (99.5% purity), Dimethyl sulfoxide (DMSO) (99.0 % purity), Lithium hydroxide (LiOH), Urea (CH_4N_2O), Sulphuric acid (98.9% purity) H_2SO_4, Acetic acid (CH_3COOH).

3.2 Experimental methods

3.2.1 Dissolution of CNC

CNC was dissolved in a solvent system consisting of 6% LiOH, 4% Urea and 90% water as shown in figure 3.1. The CNC powder (60 mg) was weighed and added to the solvent system of 6 ml and vortexed for 20 minutes. The resulting concentration of the CNC solution was 10 mg/ml. The CNC solution was then kept in the refrigerator for 48 hours to obtain a clear solution.

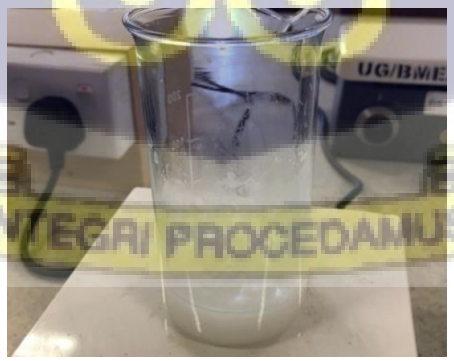

Figure 3.1: CNC powder in solvent system

3.2.2 Dissolution of HAP

The HAP powder (0.6 g) was dissolved in 60 ml of 5 % glacial acetic acid as shown in figure 3.2. The resulting mixture was stirred for 20 minutes to attain complete dissolution. The concentration of HAP obtained was 10 mg/ml.

Figure 3.2: HAP powder in 5% glacial acetic acid

3.2.3 Composite Formation

3.2.3.1 CNC as base material

Dissolved CNC solution is thawed to form a transparent solution and divided into five equal parts: 5 ml each. To each 5 ml CNC solution, varied masses of HAP (0.5 mg, 1.0 mg, 1.5 mg, and 2.0 mg) were added. The CNC solution without HAP served as a control. The resulting suspensions were vortex at a speed of 1400 rpm for 15 minutes. The HAP/CNC composite solutions were placed in a vacuum oven at 40 °C for 5 minutes. The solutions were allowed to cool and stored for 72 hours. The solution is then centrifuged at 3600 rpm for 10 minutes to obtain the HAP/CNC composites. The products are washed with distilled water and dried in vacuum to obtain dry powders of the composites.

3.2.3.2 HAP as base material.

HAP solution was divided into 5 parts (5 ml each). To each of the parts, 20 µl, 40 µl, 60 µl, and 80 µl of CNC were added. The added volumes of CNC solution represent 0.5 mg, 1.0 mg, 1.5 mg and 2.0 mg of CNC added. HAP only was used as a control in this study. The resulting mixtures were agitated for 15 minutes with the help of the vortex at a speed of 1400 rpm to obtain a uniform mixture. The mixture is then heated at 45°C for 5 minutes. The mixture is allowed to cool and stored for 72 hours. The mixture is centrifuged at 3600 rpm for 10 minutes to obtain the CNC/HAP composites. The product is washed with distilled water several times. Dry powders of the composites were obtained by drying the product in vacuum.

3.2.4 Calibration Curve of Model Drug (Curcumin)

The calibration curve developed in this study was utilized to assess the amounts of curcumin in the release medium. 8 mg of curcumin powder was dissolved in 8 ml of DMSO-water (v/v 1:1) to obtain a concentration of 1 mg/ml of the resulting solution. The solution was vortexed for 30 minutes in order to obtain a uniform solution. Subsequent concentrations were obtained through serial dilution. A calibration curve (R^2 = 0.979) was plotted by measuring the absorbance of the diluted solutions at a wavelength of 428 nm.

3.2.5 Drug Loading

Curcumin (30 mg) was dissolved in 14 ml of DMSO-water (v/v 1:1) to obtain a concentration of 2.14 mg/ml. Composites (15 mg) were weighed and transferred into Eppendorf tubes. Curcumin solution (1.5 ml) was pipetted and added to the composites (and control). The mixture was then agitated gently using the rotating equipment at 18 rpm to ensure the adsorption of the drug onto the composites as shown in figure 3.3. At predetermined times the mixture was centrifuged at 3000 rpm for 1 minute and 50 µl of the supernatant was pipetted and diluted with 950µl of 50% DMSO

solution. The absorbance of the resulting solution was measured at wavelength of 428 nm using the JENWAY 6705 UV-Vis Spectrophotometer (Antylia Scientific, USA). 50 µl of fresh 50% DMSO solution was replaced in the solution to maintain sink conditions. The drug loading was done for 22 hours.

Equation (3.1) was used to determine the amount of curcumin entrapped onto the formulated composites.

$$\text{Entrapment Efficiency (\% EE)} = \frac{x-y}{x} \times 100\% \qquad (3.1)$$

Where, x = total concentration of drug added

y = concentration of drug in the supernatant.

Entrapment efficiency estimates the percentage of the active ingredient that is adsorbed on the composites compared to the total amount of drug added.

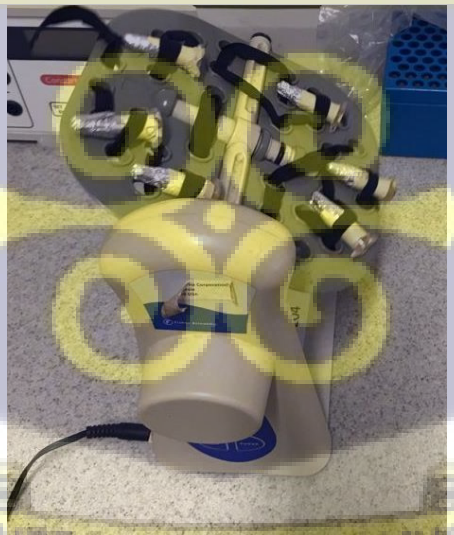

Figure 3.3: Agitation of composites in drug solution to ensure adsorption of drug onto composites.

3.2.6 *In vitro* drug release

The curcumin solution is discarded, leaving the curcumin-loaded composites in the Eppendorf tubes. 1.5 ml release medium made up of DMSO-water (v/v 1:1) at pH (≈ 6.2 and ≈ 7.4) was added to each composite and rocked on the rotating equipment at 18 rpm. At fixed time intervals, the mixture was centrifuged at 6000 rpm for 1 minute and 50 µl of the supernatant was carefully pipetted and diluted with 950 µl of 50% DMSO solution. Absorbance of the resulting solution was measured at wavelength of 428 nm using the UV-Vis Spectrophotometer. 50 µl of fresh 50% DMSO solution was replaced in the solution to maintain sink conditions. The drug release was done for 6 hours at 37 °C. The concentration of the released curcumin was determined using a standard curve of curcumin in 50% DMSO.

Technical replicates were incorporated into the experimental design to ensure reliability and reproducibility of the data. The same experimental approach was conducted in triplicates under same experimental conditions. This made it possible to evaluate measurement precision and find any potential variations or errors in the experimental design.

3.3 Material Characterization Methods

3.3.1 Fourier-Transform Infrared spectroscopy (FTIR)

FTIR is a well-established technique for chemical compound identification and structural analysis. Peaks in an infrared spectrum represent the excitation of vibrational modes of molecules in the sample and are thus associated with the various chemical bonds and functional groups present in the molecules (Nandiyanto, Oktiani, & Ragadhita, 2019). The infrared beam is focused on the sample thereby allowing various interactions with the sample. A slit selects the various wavelengths that pass through the sample at any given time. Absorption of light by the sample depends on the sample's chemical properties. A detector then collects the radiation that passes

through the sample and compares its energy to the reference. The analysis was conducted on Hydroxyapatite (HAP), Cellulose Nanocrystals (CNC) and the formulated HAP/CNC composites. The FTIR was recorded with a Nicolet MAGNA-IR 750 Spectrometer (Nicolet Instrument Co., Madison, WI, USA). The analysis was done from 450 to 4000 cm^{-1} and the data was analyzed.

3.3.2 X-ray powder diffraction (XRD)

X-ray powder diffraction is a non-destructive technique that reveals information about the crystallographic structure, physical properties, and chemical composition of materials (Jurásek, Bartůněk, Huber, & Kuchař, 2019). Constructive interference of a monochromatic beam of X-rays at different angles from each set of lattice planes in a material produces XRD peaks (Bunaciu, Udriştioiu, & Aboul-Enein, 2015). These peaks are determined by the positions of atoms within the lattice planes. This technique uses Bragg's law of diffraction. Which is defined as, $n\lambda = 2dSin\theta$, where n is the reflection order, λ is the wavelength, d is the interplanary distance and θ is the angle of reflection. XRD analysis was conducted on Hydroxyapatite (HAP), Cellulose Nanocrystals (CNC) and the formulated HAP/CNC composites. The XRD spectra of samples were obtained by an Analytical diffractometer with CuKα radiation operated at 40 mA and 45 kV. Samples were scanned from 5° to 100° with a scan step size of 0.05° and a scan step time of 38.5 seconds.

3.3.3 Ultraviolet-visible spectroscopy (UV-VIS)

UV-vis spectroscopy is used to determine the absorbance spectra of a compound in solution. It works based on Beer-Lambert law as seen in equation (3.2) which states that there is a linear relationship between the concentration and the absorbance of the solution.

$$A = \varepsilon \times b \times c \qquad (3.2)$$

where, A is the absorbance, ε is the molar absorptivity of the solution, b is the path length of the cuvette which is usually 1 cm, and c is the concentration of the solution.

A source of light is needed to emit light over a wide range of wavelengths. Since the UV-vis spectrophotometer measures absorbance in the ultraviolet and visible region, a source of light that measures both UV and visible light ranges is appropriate. An example of a source of light that exhibits such a characteristic is the xenon lamp. However, xenon lamps are less stable and very expensive. Therefore, tungsten or halogen lamps and deuterium lamps are used. Tungsten or halogen lamp is used for measurement in the visible light range, while deuterium lamp is used for the UV range. Since two sources of light are used, there is a switchover when measurements are across the UV and visible ranges. The incoming light is split into a narrow band of wavelengths by a monochromator. The selected wavelength then passes through the sample. Measuring a reference sample is essential for all analyses.

In this work, the upload and release rates were studied using the UV-vis spectrophotometer. It helps to determine the amount of drugs that was adsorbed onto the formulated composites and the amount of drugs released from the loaded composites by measuring the absorbance within a specific time interval. The JENWAY 6705 UV-vis spectrophotometer was used for UV-vis characterization. The samples were measured at a wavelength of 428 nm. OriginPro 8.5 (OriginLab Corp., Northampton, MA, USA) was used to analyze the data obtained from the absorbance measurements.

3.4 Cell viability studies

Biocompatibility is one of the key properties of bio-ceramic and human biological system and this is assessed by performing in vitro cell viability assays (Williams, 2014). In this study, commercial HAP and formulated composites were assessed by utilizing MTT assay to evaluate the viability of MDA-MB-231 cells on various formulated composites. A percentage of cell viability greater than 90% indicates that the sample is biocompatible to MDA-MB-231 cells.

3.4.1 Cell culture conditions

Prior to experiments, MDA-MB-231 cells were cultured in Dulbecco's modified Eagle's medium (DMEM; Life Technologies Corporation, Grand Island, NY, USA) with 10% fetal bovine serum (FBS; R&D Systems, Minneapolis MN, USA), 1% penicillin and streptomycin (Life Technologies Corporation, Grand Island, NY, USA) in a humidified 5% CO_2 environment at 37 °C (cell culture incubator). Confluent cell monolayers were detached from the culture flask with 2ml of 1x trypsin-EDTA solution (Gibco, Waltham, MA, USA), suspended in culture medium and incubated for 5 minutes for subculturing. The trypan blue exclusion experiment was used to measure cell viability and density.

3.4.2 MTT (3-(4, 5-dimethylthiazolyl-2)-2, 5-diphenyltetrazolium bromide) assay

MTT assay was used to test curcumin's anticancer activity. The MTT assay is based on the ability of cells to convert the yellow soluble salt of MTT (3-(4,5-dimethylthiazol-2-yl)-2,5-diphenyltetrazolium bromide) to an insoluble formazan (purple-blue) precipitate. MDA-MB-231 (10,000 cells/100 µL) cells were seeded overnight in 96-well plates. Prior to testing loaded composites on cells, 2.5 µL of raw composites (composites without curcumin) and HAP in 5% DMSO were tested on cells to assess compatibility and viability of the samples with the cell culture system. This is done to determine if the samples are toxic to cells and to assess baseline effects.

MDA-MB-231 cells were then treated with 2.5 µL of loaded composites in 5% DMSO and incubated for 48 hours. After the incubation period, 20 µL of MTT was added to each well and incubated for further 4 hours after which 100 µL of acidified isopropanol was added to dissolve the MTT. A microplate reader spectrophotometer was used to record the optical densities at 570 nm after 30 minutes of incubation.

3.5 Data analysis

Data were obtained from the drug loading and release experiments. The XRD and FTIR test generated data in the form of spectra. Origin Pro software was employed for the analysis of the XRD and FTIR spectra and cell viability studies. The data obtained from the drug release were tested for normality using Kolmogorov-Smirnov test. Data showing $p > 0.05$ were accepted to be normally distributed, hence parametric test was performed on the data. One-way analysis of variance (ANOVA) was used to find out whether there were statistically significant differences in the release data with respect to the synthesis of composites and cumulative release in different pH release media. Tukey test was used to find out the means that were significantly different from each other at $p < 0.05$. The drug release data was fitted using the Higuchi and Korsmeyer-Peppas models and cubic degree polynomial. A higher regression coefficient (R^2) indicated a strong correlation and improved linearity. Origin Pro software was used to determine the Coefficients of Determination when fitting the data to the different models. These kinetic models provide insights into the underlying mechanism of drug release. The Higuchi model is based on diffusion. It describes drug release from insoluble matrix dependent on the square root of time. This model hypothesizes that the initial concentration of drug in the matrix is higher than the solubility of the drug. Korsmeyer-Peppas model is used to ascertain the type of diffusion taking place. This is

characterized by the diffusion coefficient factor, (n) in the Korsmeyer-Peppas equation as shown in table 4.5.

CHAPTER FOUR

4.0 Results and Discussion

This chapter presents and discusses the experimental and characterization outcomes of the modified HAP/CNC composites.

4.1 Fourier-transform infrared spectroscopy (FTIR)

4.1.1 Composites with CNC as base material

The FTIR spectra of the HAP, CNC and the HAP/CNC composites are presented in figure 4.1. The FTIR spectral data are used to study the changes that occurred in the functional groups of CNC when reacted with HAP.

The distinct transmission peaks of CNC were observed at the wavenumbers of 3566, 3354, 1625, 1009 cm^{-1}. For HAP, the distinct transmission peaks were at 1029, 601 and 565 cm^{-1}. 3566 and 3354 cm^{-1} bands are attributed to -OH intramolecular hydrogen bonding (Fan, Dai, & Huang, 2012) present in CNC. 1625 cm^{-1} indicates C-H symmetrical stretching (Terpáková, Kidalová, Eštoková, Čigášová, & Števulová, 2012) and 1009 cm^{-1} is attributed to C–O Stretching vibration at the crystalline region of cellulose (Abidi et al., 2008). 1029 and 601 cm^{-1} of HAP indicate PO_4^{3-} Stretching (Varma & Babu, 2005) and PO_4^{3-} Bending (Yusufoglu & Akinc, 2008) respectively. 565 cm^{-1} is attributed to P-O symmetric stretching of PO_4 group (Varma & Babu, 2005). The weak peak present at 875 cm^{-1} is ascribed to bending in the CO_3^{2-} ions (Berzina-Cimdina & Borodajenko, 2012). It can also be attributed to the presence of HPO_4^{2-} (Gozalian, Behnamghader, Daliri, & Moshkforoush, 2011). After the modification of CNC with varied masses of HAP, two shoulders 3443 and 3215 cm^{-1} corresponding to OH Stretching (Kallel et al., 2016) and -OH due to intermolecular hydrogen bonding, reduced. The peak at 3696 cm^{-1} which is attributed to –OH

intramolecular hydrogen bonding (Fan et al., 2012) was enhanced in all composites except 2 mg HAP/CNC composite. The peak at 3566 cm^{-1} reacted when HAP was added and moved to a higher wavenumber of 3622 cm^{-1}. However, the peak at 3622 cm^{-1} was not distinct in the 2 mg HAP/CNC composite. The broad region at 2911 – 2871 cm^{-1} which indicates the presence of CH Stretching (Schwanninger, Rodrigues, Pereira, & Hinterstoisser, 2004) was absent in the 1.5 mg HAP/CNC composite (it was weakened and disappeared), and was reduced in the 1 mg HAP/CNC composite and enhanced in the rest of the composites. After modification, the peak at 1420 cm^{-1} which represents the amount of crystalline structure of cellulose (Åkerholm, Hinterstoisser, & Salmén, 2004) increased with the amount of HAP added to the composite. However, the 2 mg HAP/CNC composite increased but did not follow that trend. The increase in the peak may be due to the mass of HAP added to CNC which might have affected the crystallinity of the resulting composite. There was also the emergence of two peaks at 911 and 863 cm^{-1} in all the composites. All composites show an increase in the peak intensity of 911 cm^{-1} which is ascribed to the interactions between glycosidic linkages and glucose units of cellulose. The peak at 1029 cm^{-1} was present in all composites. However, it was broadened and moved to a lower wavenumber for all the composites except that of the 2 mg HAP/CNC composite. This could be due to the presence of hydrogen bonding during the modification of CNC with HAP.

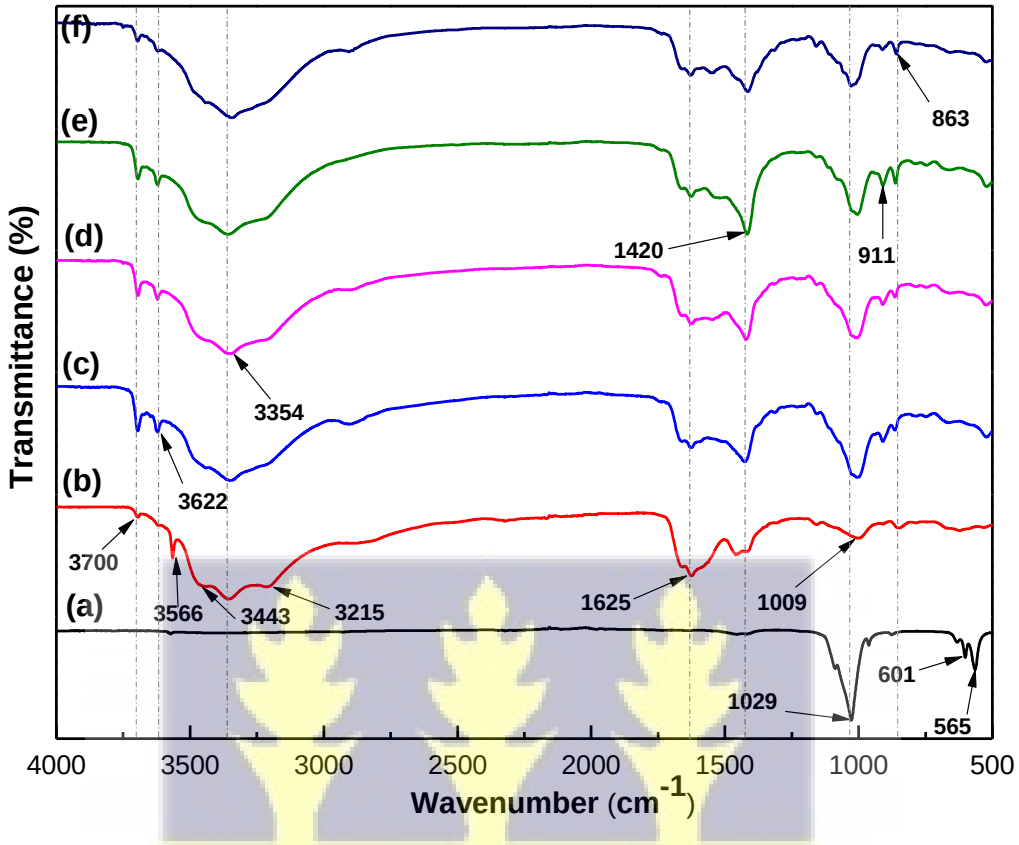

Figure 4.1: FTIR spectra of (a) HAP Only (b) CNC Only (c) 0.5 mg HAP/CNC (d) 1.0 mg HAP/CNC (e) 1.5 mg HAP/CNC (f) 2.0 mg HAP/CNC composites where CNC is the base material.

4.1.2 Composite using HAP as base material.

The distinct transmission peaks of HAP only were observed at wavenumbers of 1740 cm^{-1}, 1366 cm^{-1}, 1028 cm^{-1}, 601 cm^{-1} and 565 cm^{-1} as shown in figure 4.2. The peak position at 1740 cm^{-1} is C=O stretching vibrations (Predoi et al., 2018), 1366 cm^{-1} represents C–O stretching vibrations (Predoi et al., 2018). Peaks at wavenumbers 1028 cm^{-1} and 601 cm^{-1} of HAP represent PO_4^{3-} stretching (Varma & Babu, 2005) and PO_4^{3-} Bending (Yusufoglu & Akinc, 2008) respectively. The peak at 565 cm^{-1} indicates P-O symmetric stretching of PO_4 group (Varma & Babu, 2005). FTIR spectra labelled 'c', 'd', 'e' and 'f' represent modified HAP with varied masses of CNC (0.5

mg, 1.0 mg, 1.5 mg and 2.0 mg). After modification, there was appearance of the peak at 3566 cm^{-1} on all the modified samples which indicates OH intramolecular hydrogen bonding in CNC (Fan et al., 2012). The peak positions 1740 cm^{-1}, 1366 cm^{-1} and 1217 cm^{-1} disappeared in all modified samples. The peak at 962 cm^{-1} which is attributed to the $(PO_4)^{3-}$ symmetric stretching (El Khouri, Zegzouti, Elaatmani, & Capitelli, 2019) present in HAP became relatively intense in all the composites. The appearance of 3566 cm^{-1}, disappearance of various peaks and increase in intensity of 962 cm^{-1} confirms the modification of HAP.

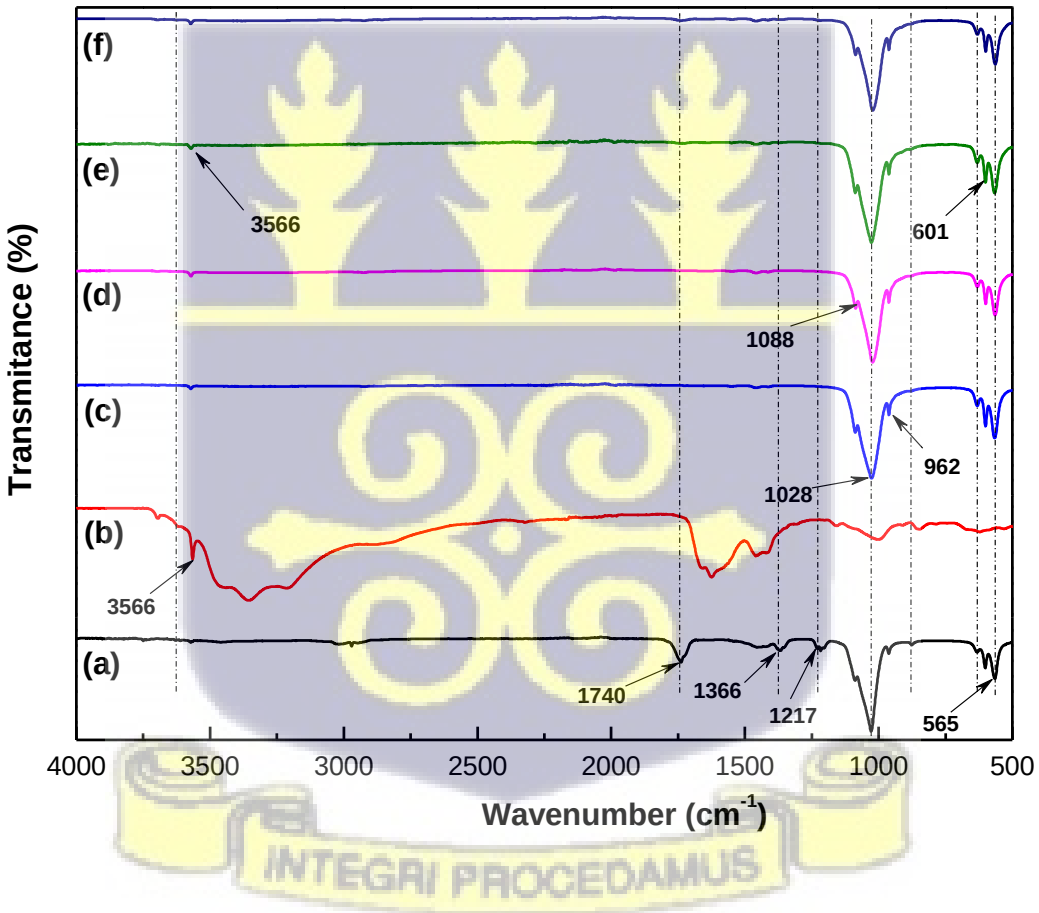

Figure 4.2: FTIR spectra of (a) HAP Only (b) CNC Only (c) 0.5 mg CNC/HAP (d) 1.0 mg CNC/HAP (e) 1.5 mg CNC/HAP (f) 2.0 mg CNC/HAP composites where HAP is the base material.

4.2 X-Ray Diffraction (XRD)

4.2.1 Composites with CNC as base material

Figure 4.3 shows the XRD pattern of HAP, CNC and HAP/CNC composites. HAP shows intense peaks at 2θ = 25.79, 31.67, 32.0, 32.79 corresponding to (002), (211), (300) and (002) which clearly indicates the presence of phosphate groups. CNC shows intense peaks at 2θ = 21.23, 22.13, 29.34, 30.46, 31.67, 64.85, 80.0 which correspond to (110), (110), (111), (202), (002), (-114) and (041). The spectra labelled 'c', 'd', 'e' and 'f' represent the XRD patterns of the CNC/HAP composites. Similar XRD patterns were observed for the composites. However, there was disappearance of the peak at 22.13° 2θ position in 0.5 mg HAP/CNC and 1.0 mg HAP/CNC composites but it reduced in the 2.0 mg HAP/CNC composite. There was a preferred orientation in 1.5 mg HAP/CNC composite of peaks at 21.23° 2θ and 22.13° 2θ. The peaks at 22.13° 2θ disappeared on addition of 0.5 mg and 1.0 mg of HAP. However, when 1.5 mg HAP was added, the peak at 22.13° 2θ increased as compared to that of CNC only and when 2.0 mg HAP was added, it decreased. The peaks at 29.34° 2θ, decreased for all composites. These changes confirm the formation of composites. The crystallinity of CNC and the composites where major changes occurred are presented in table 4.1.

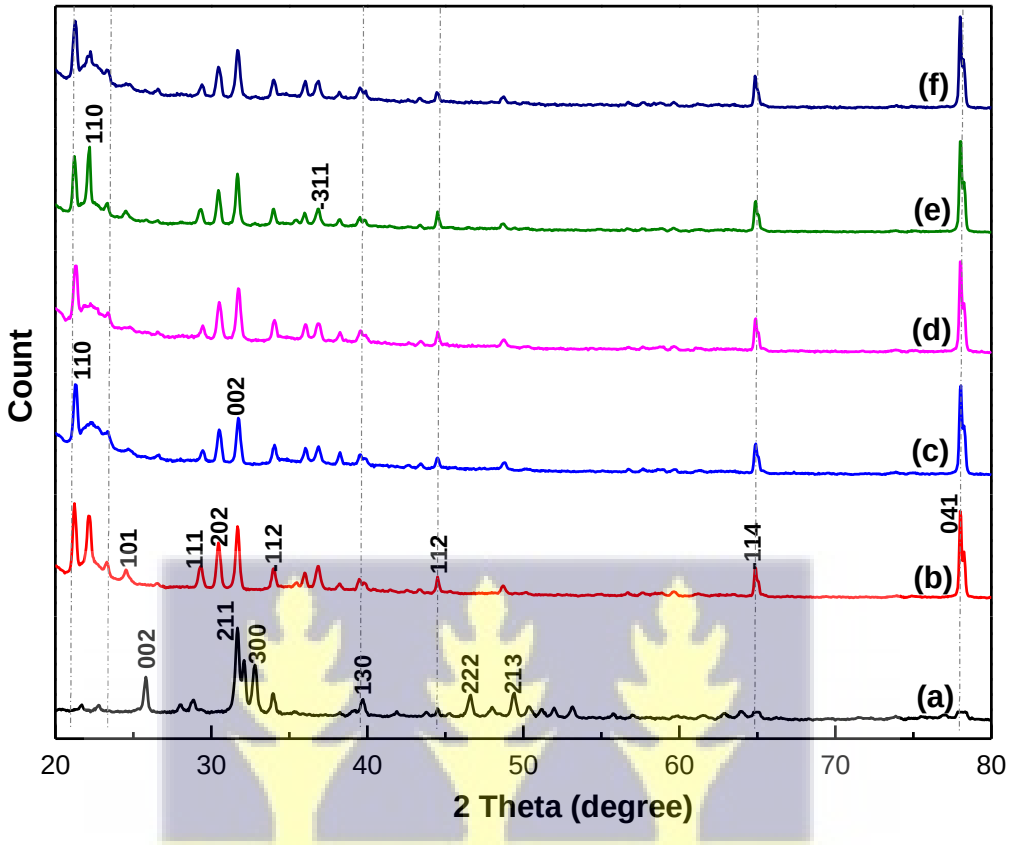

Figure 4.3: XRD plot of (a) HAP Only (b) CNC Only (c) 0.5 mg HAP/CNC (d) 1.0 mg HAP/CNC (e) 1.5 mg HAP/CNC (f) 2.0 mg HAP/CNC composites where CNC is the base material.

Table 4.1: Crystallinity of samples in the range 20° – 25° 2θ

Samples	Crystallinity (%)
CNC Only	49
0.5 mg HAP/CNC	43.6
1.0 mg HAP/CNC	39.6
1.5 mg HAP/CNC	41.4
2.0 mg HAP/CNC	41.7

4.2.2 Composites with HAP as base material

Figure 4.4 shows the XRD pattern of HAP, CNC and CNC/HAP composites. HAP shows peaks at 2θ= 25.79 °, 31.67 °, 32.0 °, 32.79 °, 33.95 ° corresponding to (002), (211), (112), (300) and (202) clearly indicate the presence of phosphate groups. Similar XRD patterns were observed for all composites. 0.5 mg CNC/HAP composite showed a decrease in major peaks of HAP including peaks at 46.72° 2θ and 49.48° 2θ corresponding to (222) and (213) however there was emergence of a peak at 49.48° 2θ and this is due to the interaction of HAP with CNC. The peak at 64.82 ° 2θ position increased more in 0.5 mg CNC/HAP than the rest of the composites. The intensity of peak at 78 ° 2θ which indicates the presence of CNC in the composites increased in 0.5 mg CNC/HAP composite but decreased in the other composites. The XRD plot clearly indicates the formation of composites. The crystallinity of HAP and the composites are presented in table 4.2.

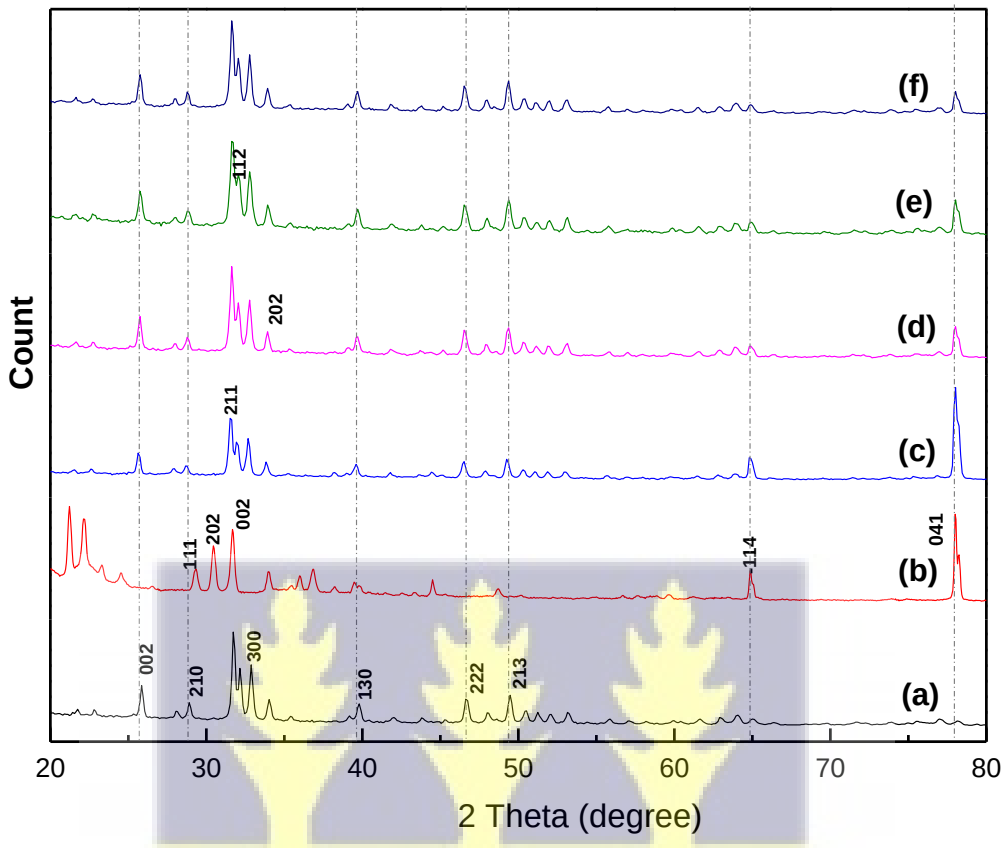

Figure 4.4: XRD plot of (a) HAP Only (b) CNC Only (c) 0.5 mg CNC/HAP (d) 1.0 mg CNC/HAP (e) 1.5 mg CNC/HAP (f) 2.0 mg CNC/HAP composites where HAP is the base material.

Table 4.2: Summary of crystallinity of samples

Samples	Crystallinity (%)
HAP Only	38.5
0.5 mg HAP/CNC	30
1.0 mg HAP/CNC	32.6
1.5 mg HAP/CNC	27.1
2.0 mg HAP/CNC	33

4.3 Standard calibration curve of model drug (curcumin)

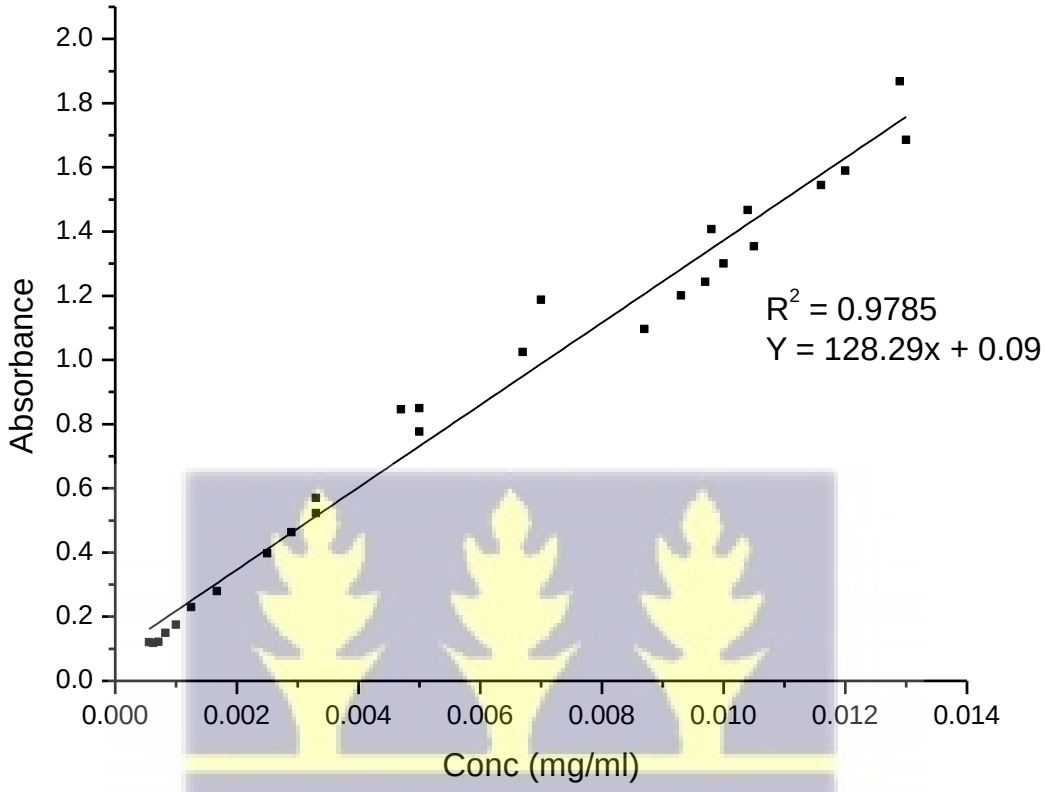

Figure 4.5: A standard calibration curve of curcumin

Figure 4.5 depicts the standard calibration curve used to determine the concentration of the drug during UV-Vis characterization. Calibration curve is plotted using known concentrations, enabling the estimation of drug concentration based on absorbance values during both drug loading and release.

4.4 Drug loading

Drug loading efficiency onto the HAP/CNC composites were determined using equation (3.1). Figure 4.6 shows absorbance against time of composites with CNC as base material and CNC only. From the graph it is observed that composites with CNC as base material and CNC (control) did not upload the model drug. From literature, CNC cannot upload hydrophobic drugs, however when CNC is modified with polymers or inorganic materials, it tends to load hydrophobic drugs. Even though in this study CNC was modified with varying masses of HAP, the resulting composites did not upload drug. This could be due to the ratio of HAP to CNC used in the composite formation. Figure 4.7 shows absorbance against time of composites with HAP as base material and HAP only. It can be observed from the graph that composites with HAP as base material and modified with varying masses of CNC uploaded the drug. The loading values of the composites (with HAP as base material) are summarized in table 4.3 below. From the table, it can be inferred that after drug loading, all composites together with the control loaded almost the same amount of drug. There was no significant difference between the samples loaded ($p > 0.05$). This could be due to the ratio of dissolved CNC and HAP used for the composite formation.

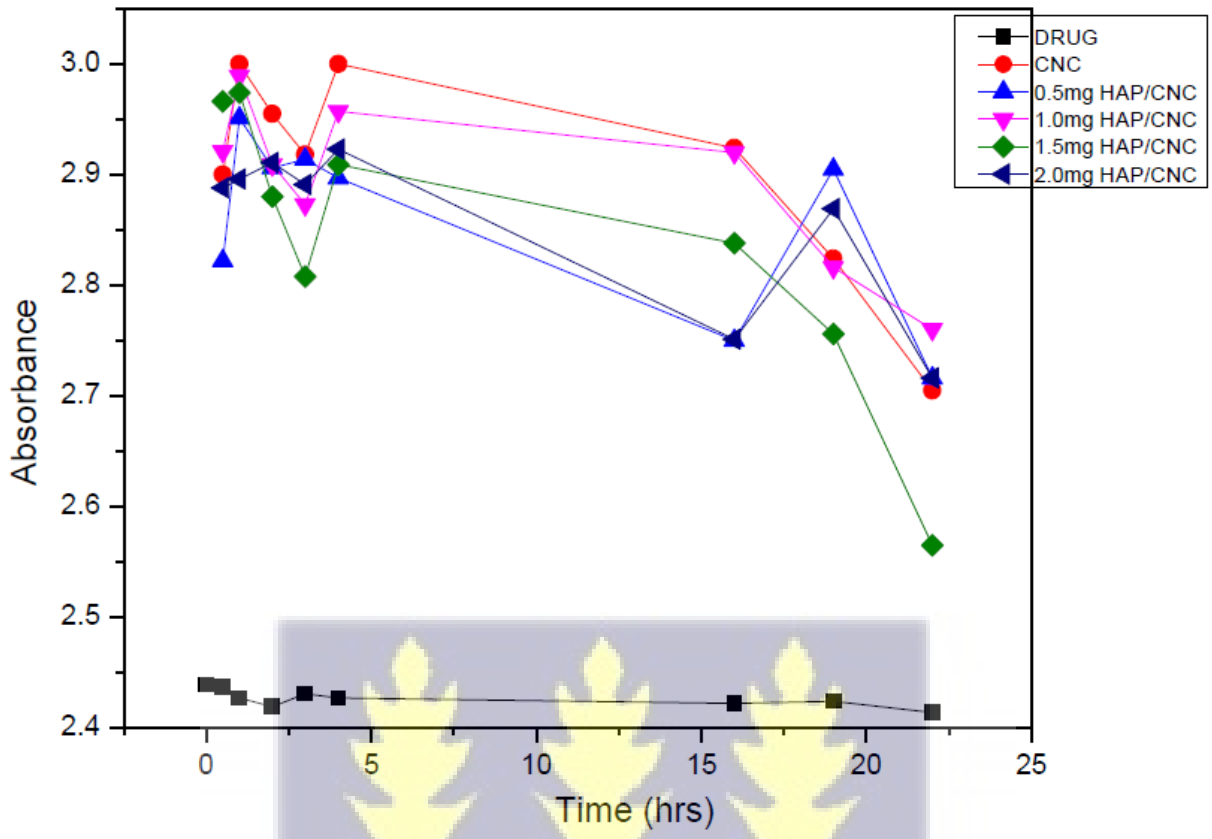

Figure 4.6: Drug upload on CNC and composites with CNC as base material

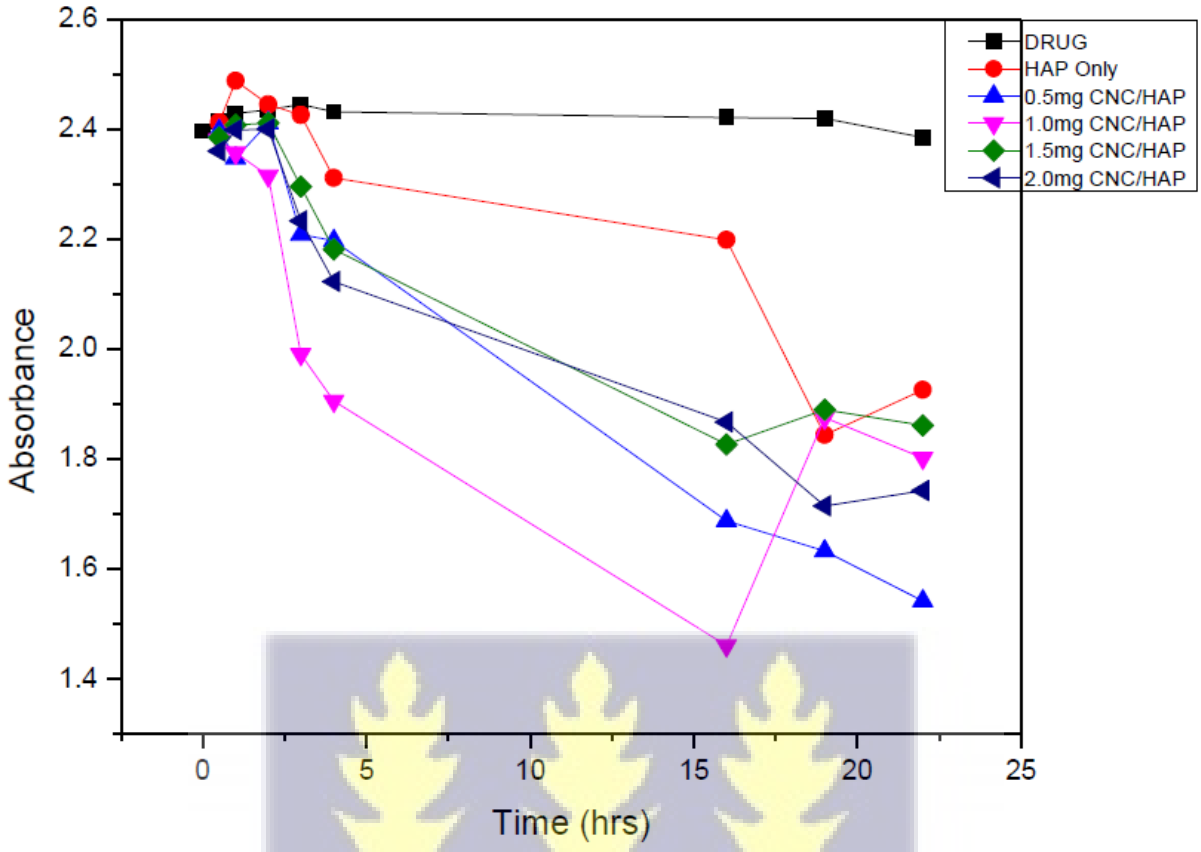

Figure 4.7: Drug upload on HAP and composites with HAP as base material

Table 4.3: Entrapment efficiency of composites with HAP as base material

Composites	Entrapment Efficiency (%)
HAP Only	84
0.5 mg CNC/HAP	85
1.0 mg CNC/HAP	86
1.5 mg CNC/HAP	86
2.0 mg CNC/HAP	85

4.5 Drug release characteristics

The drug release profiles of curcumin from composites with HAP as base material in 50 % DMSO at different pH values are shown in figures 4.8 and 4.9 below. Loaded composites were suspended in 50 % DMSO, centrifuged and the drug (curcumin) content present in the supernatant was quantified by UV-Vis spectrophotometer. The drug release profiles showed that the release of curcumin from all the formulated composites in pH ≈ 6.2 was higher than pH ≈ 7.4. The cumulative release of curcumin from the composites at different pH values after 6 hours is shown in table 4.4.

Table 4.4: Percentage cumulative release of curcumin from composites

	% Cumulative release of drug in different pH	
Composites	**pH 6.2**	**pH 7.4**
HAP Only	35.36±0.52	27.95±2.38
0.5 mg CNC/HAP	32.87±1.20	18.99±0.23
1.0 mg CNC/HAP	29.89±4.87	16.52±0.83
1.5 mg CNC/HAP	33.78±2.73	23.32±0.38
2.0 mg CNC/HAP	32.14±5.14	19.60±0.16

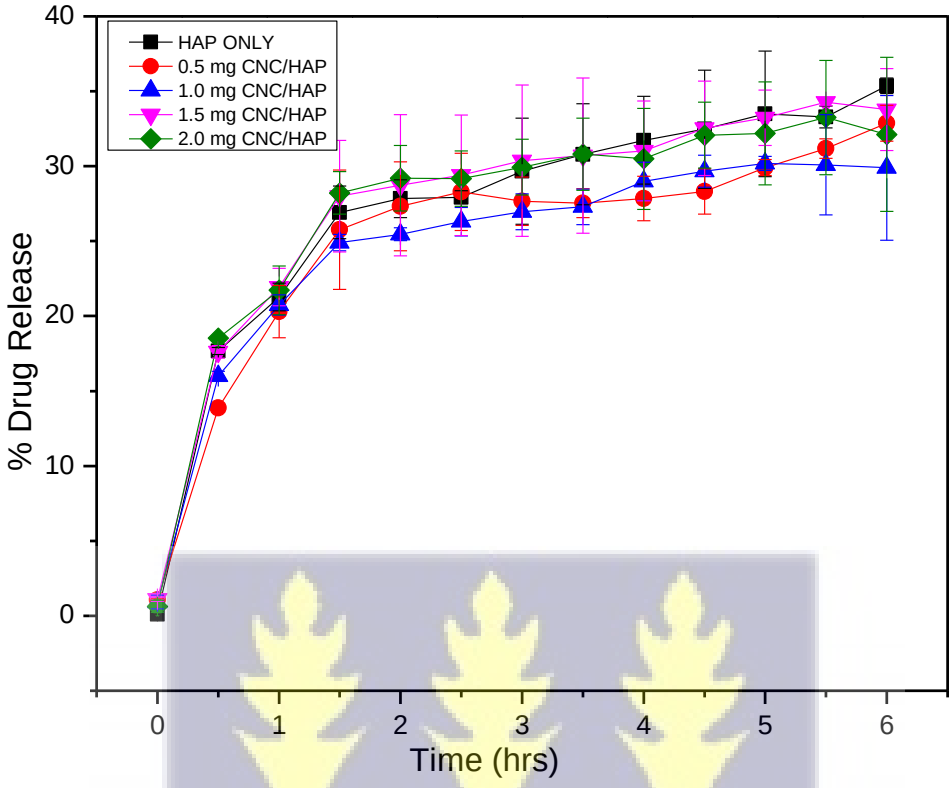

Figure 4.8: Drug release profiles for samples in acidic medium (pH ≈ 6.2)

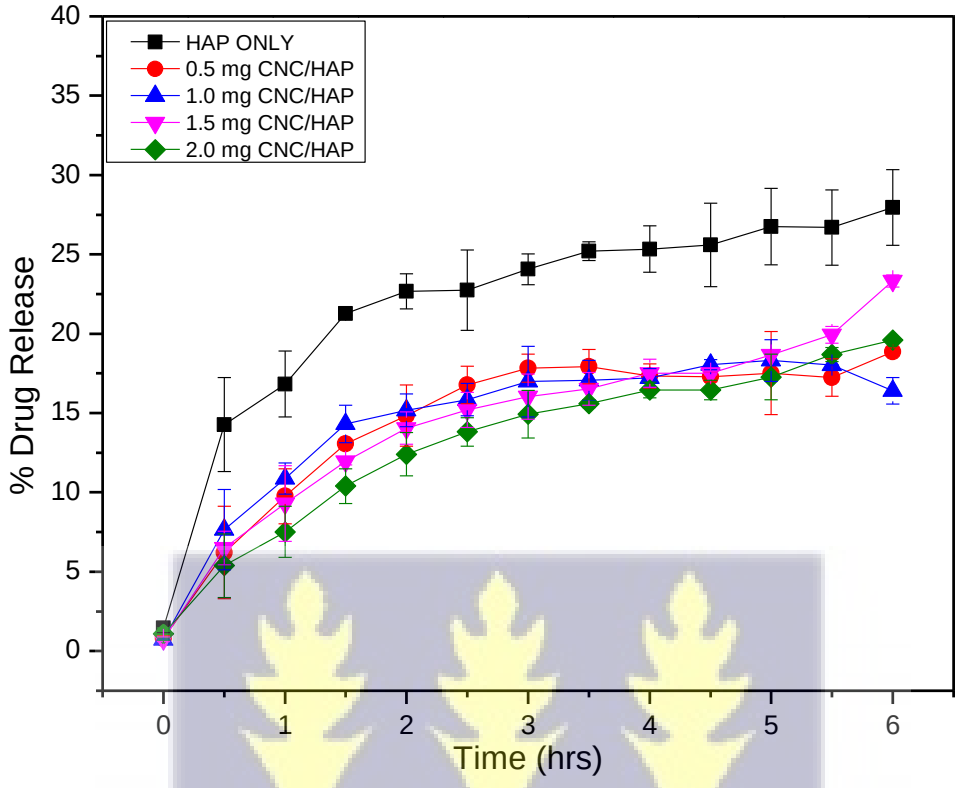

Figure 4.9: Drug release profiles for samples in neutral medium (pH ≈ 7.4)

There was a higher amount of drug released acidic medium (pH ≈ 6.2) than in neutral medium (pH ≈ 7.4). This could be because excess hydrogen ions present in the acidic release medium readily broke the hydrogen bonds that hold the drug onto the composites. From the release profiles, the release of the drug (curcumin) from the control (HAP Only) after 6 hours was found to be the highest in both release media (pH ≈6.2 and pH ≈7.4), 35.36±0.52 % in acidic pH and 27.95± 2.38% in neutral pH. The percentage cumulative drug release was higher in pH 6.2 than in pH 7.4 for all corresponding samples. There was a sustained release of all samples in pH 7.4. (0.5 mg, 1.0 mg, 1.5 mg and 2.0 mg) CNC/HAP composites released 18.99± 0.23%, 16.52±

0.83%, 23.32± 0.38% and 19.60± 0.16% of the drug respectively. It is observed that there is a rapid release of curcumin from all samples in pH 6.2 release media. This could be because, in acidic medium, the introduction of H^+ ions readily break the bonds between the curcumin and the composites, hence, facilitated the initial high release of curcumin during the 30th minute. The effect of ionic interaction was more in the acidic release medium where carboxylic group is dissociated than in neutral pH.

The amount of drug released for 6 hours in pH 7.4 release medium is in the order HAP Only > 1.5 mg CNC/HAP > 2.0 mg CNC/HAP > 0.5 mg CNC/HAP > 1.0 mg CNC/HAP. Whereas the amount of drug released in pH ≈ 6.2 is in the order HAP Only > 1.5 mg CNC/HAP > 0.5 mg CNC/HAP > 2.0 mg CNC/HAP > 1.0 mg CNC/HAP

One-way independent analysis of variance (ANOVA) showed that there was significant difference between the means of the rate of drug release of the composites in pH ≈ 7.4 ($p = 0.004$). Tukey post hoc test showed that the drug release rate was significant between all the composites and the control, HAP only. When 0.5 mg, 1.0 mg, 1.5 mg and 2.0 mg CNC were added to HAP, it reduced the percentage release rate significantly (18.99± 0.23%, $p = 0.020$; 16.52± 0.83%, $p = 0.023$; 23.32± 0.38%, $p = 0.024$; 19.60± 0.16%, $p = 0.004$). These results show that the addition of CNC affected the drug release in pH 7.4. However, there was no significant difference between the composites ($p > 0.05$).

One-way ANOVA showed that there was a significant difference between the means (three replicates) of the drug release rate across groups (samples in pH ≈ 6.2 and pH ≈ 7.4) ($p < 0.001$). Tukey test showed that the drug release rate was significant between all the composites ($p < 0.05$) across group except the control, HAP where there was no significant difference ($p = 0.7581$). This

reveals that the change in pH affected the drug release in the composites. However, this is not the case in control, HAP.

4.6 *In vitro* drug release kinetics

In order to predict the release behavior of a solute from a nanocomposite or material, the release data must fit a mathematical model. Regression coefficient (R^2) values shows the relationship between the drug release and the time of release. The kinetic models explain the mechanism of drug release from the samples. Figures 4.10, 4.11 and 4.12 show how the release data were fitted to the models and cubic degree polynomial. Table 4.5 shows a summary of the R-squared and constants from the fitted models. From the table, it can be observed that the 2.0 mg CNC/HAP composite in pH ≈7.4 release media showed the highest correlation with Higuchi model (R^2 = 0.9831). The correlation coefficient of HAP only in pH ≈ 6.2 release media was the highest with Korsmeyer-Peppas model (R^2 = 0.9898). The cubic degree polynomial is not a function of time, so it was not used to show correlation and linearity. It only gives an idea as to how many factors are involved to achieve the release rate of the drug.

4.6.1 Drug release in pH ≈ 6.2

There was a higher correlation with the Korsmeyer-Peppas model than the Higuchi model for all the samples. HAP showed the highest correlation in both models (R^2 = 0.9898 for Korsmeyer-Peppas) and (R^2 = 0.8138 for Higuchi). Amongst the composites, 0.5 mg CNC/HAP composite showed the highest correlation (R^2 = 0.7571) as far as Higuchi model is concerned. Between the composites, 1.0 mg CNC/HAP composite exhibited the highest correlation (R^2 = 0.9828) for Korsmeyer-Peppas model. There was not much of a difference between the correlation coefficient for Korsmeyer-Peppas model for all samples. Table 4.5 gives a summary of the R-squared of the

various data. One-way independent analysis of variance (ANOVA) revealed that the various masses of CNC did not have any significant influence on the rate of drug release ($p = 0.894$).

4.6.2 Drug release in pH ≈ 7.4

There was also a higher correlation with the Korsmeyer-Peppas model than the Higuchi model for all the samples in neutral pH. 2.0 mg CNC/HAP composite showed the highest correlation ($R^2 = 0.9831$) with Higuchi model. HAP exhibited the highest correlation ($R^2 = 0.9838$) with Korsmeyer-Peppas model, followed closely by 2.0 mg CNC/HAP composite ($R^2 = 0.9835$) and 1.5 mg HAP/CNC composite ($R^2 = 0.9753$). Between the composites, 2.0 mg CNC/HAP composite ($R^2 = 0.9835$) exhibited the highest correlation for Korsmeyer-Peppas model followed closely by 1.5 mg CNC/HAP composite ($R^2 = 0.9753$). Table 4.5 gives a summary of the R-squared of all samples.

Korsmeyer-Peppas model characterizes its release mechanism by the diffusion coefficient factor (n). The values of the diffusion coefficient factor (n) from table 4.5 is less than 0.45 for all samples, which indicate that the drug release followed Fickian diffusion. Fickian diffusion refers to the diffusion of a substance due to concentration gradient. Hence the rate of drug release from the samples is proportional to the concentration gradient of the drug. 1.0 mg, 1.5 mg and 2.0 mg CNC/HAP composites in acidic medium (pH ≈ 6.2) exhibited the same release mechanism. However, the percentage drug release for these composites was slightly lower than the control (HAP only). This could be as a result of the presence of excess H^+ ions present in the acidic release medium.

All synthesized composites followed the Korsmeyer-Peppas and Higuchi models. The cubic degree polynomial suggests that the drug release was based on three factors. The three factors could be the concentration gradient of the drug, diffusion distance of the drug from the composite to the release environment and the surface area of the composite.

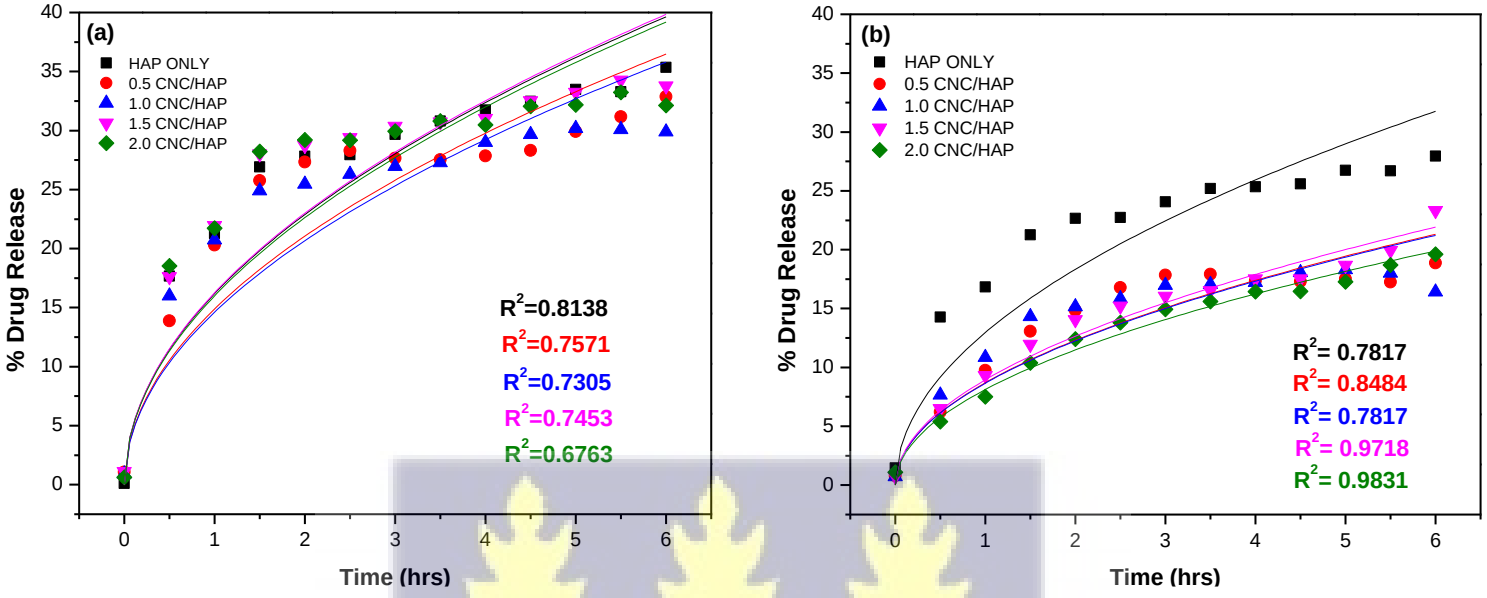

Figure 4.10: Higuchi release profile for all samples in (a) pH ≈ 6.2 and (b) pH ≈ 7.4

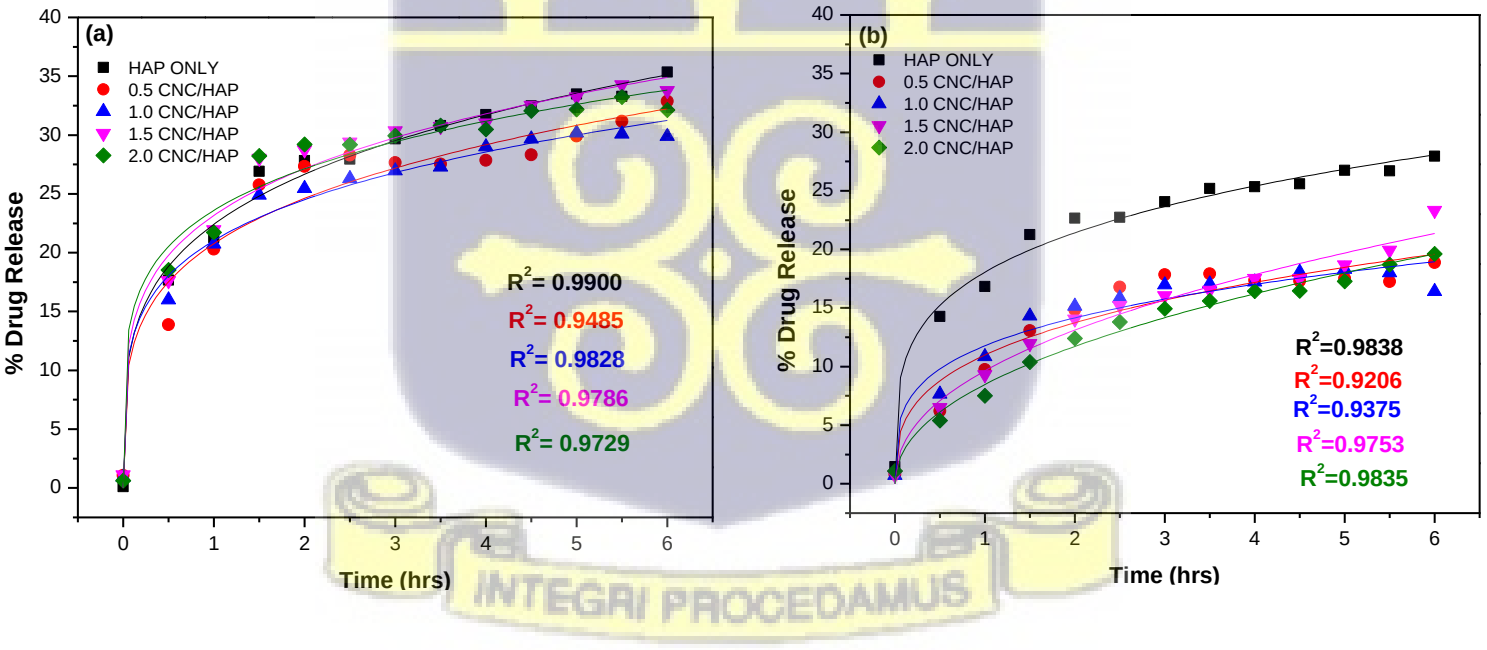

Figure 4.11: Korsmeyer-Peppas release profile for all samples in (a) pH ≈ 6.2 and (b) pH ≈ 7.4

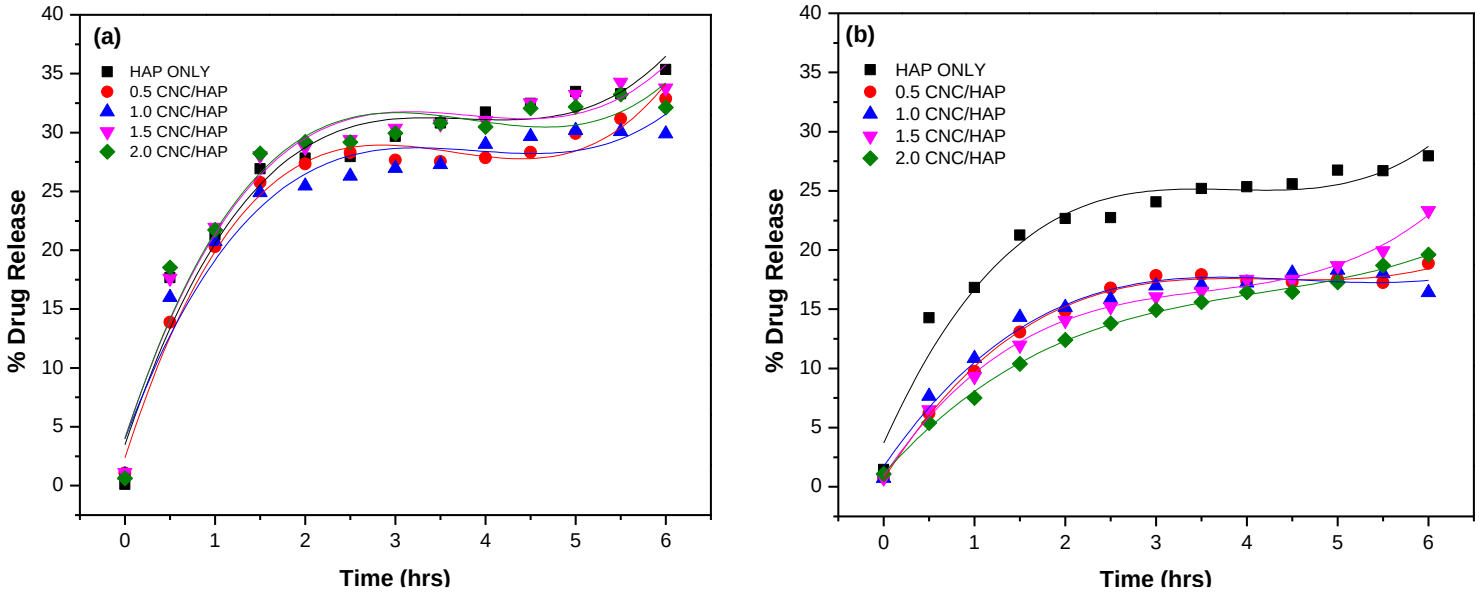

Figure 4.12: Cubic degree polynomial release profile for all samples in (a) pH ≈ 6.2 and (b) pH ≈ 7.4

Table 4.5: R-squared values from fitted models.

Kinetic Model	Equation	Parameter	HAP Only		0.5 mg CNC/HAP		1.0 mg CNC/HAP		1.5 mg CNC/HAP		2.0 mg CNC/HAP	
			6.2	**7.4**	**6.2**	**7.4**	**6.2**	**7.4**	**6.2**	**7.4**	**6.2**	**7.4**
Higuchi	Log Q = log k + 1/2 log t	R^2	0.8138	0.7817	0.7571	0.8484	0.7305	0.7817	0.7453	0.9718	0.6764	0.9831
		k	16.1842	12.9652	14.8901	8.6990	14.6178	8.6615	16.2654	8.9471	15.9976	8.1214
Korsmeyer -Peppas	Log Q = Log k + n Log t	R^2	0.9898	0.9838	0.9485	0.9206	0.9828	0.9375	0.9786	0.9753	0.9729	0.9835
		k	22.4101	18.0574	20.7692	10.9891	21.0280	11.7755	23.1658	9.6433	23.6014	8.4751
		n	0.2507	0.2462	0.2453	0.3226	0.2208	0.2656	0.2287	0.4436	0.2009	0.4380

4.7 Cell viability

According to figure 4.13, the MTT assay results showed percentages greater than 90%, indicating that all composites and commercial HAP had a positive interaction with MDA-MB-231 cells in terms of cell proliferation, demonstrating their non-toxic nature. Curcumin was then uploaded on the CNC/HAP composites with HAP as control and released for 9 hours to see the effect of the loaded composites on the breast cancer cells (MDA-MB-231 cells). CNC/HAP composite (2.0 mg) was chosen for the experiment because it is comparable to HAP only, both of which had 667.5% and 666.1% percentage increase in cell growth respectively.

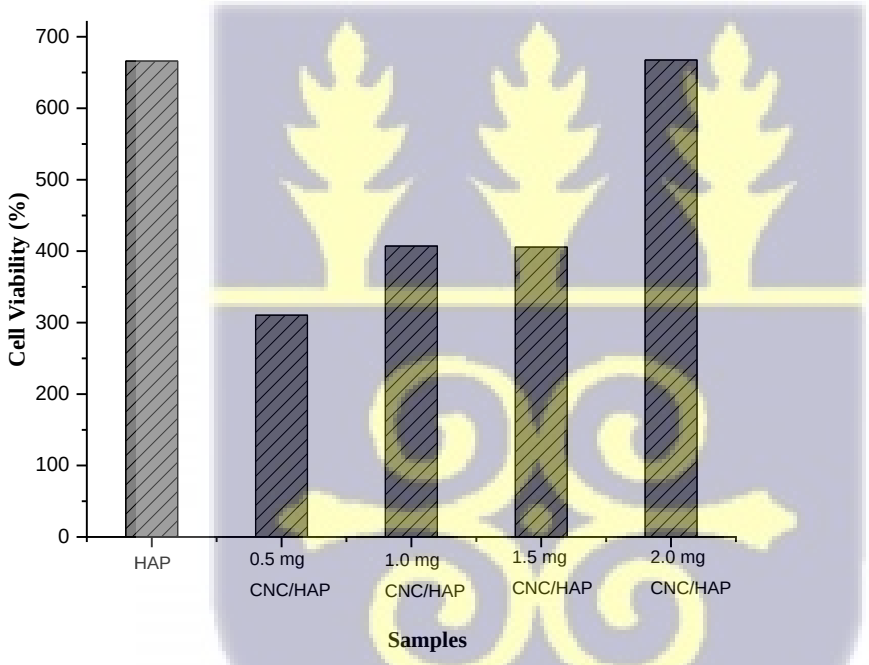

Figure 4.13: Cell viability of all composites and control using MTT assay.

From figure 4.14, it can be observed that from the first to the ninth hours, the cell viability of the 2.0 mg CNC/HAP composites is lower than it was at time zero. This indicates that the drug released from the composite during the time interval (9 hours) inhibited the growth of MDA-MB-231 cells. Cell viability percentage decreased from 77.51% at the beginning of the experiment (at time zero) to 41.84% after one hour (at 1 hour), it then increased steadily to 59% at the ninth hour. This indicates that curcumin was released in a controlled manner from the 2.0 mg CNC/HAP composite which was used as a drug carrier throughout the experiment. From figure 4.15, the percentage cell viability at the second hour (21.43%) indicates a burst release of the curcumin from HAP only. This phenomenon compromises the effectiveness of treatment as drug is lost in an uncontrolled manner and there may lead to disease relapse as a result. From figure 10, the percentage cell viability showed a fluctuating form. This confirms the nature in which HAP behaves as a drug carrier; sorption, where the release is driven by continuous concentration gradient which is generated within the HAP as a carrier and the physiological microenvironment of the cell media. This makes HAP not to have a controlled release of the drug (curcumin). The cell viability fluctuates during the nine-hour release period. In general, the metabolic activity of MDA-MB-231 cells in the presence of loaded HAP only was higher than that of 2.0 mg CNC/HAP composite.

It can be inferred from the results obtained that combining HAP and cellulose was not harmful to MDA-MB-231 cells and may serve as a better option for a drug carrier than HAP only. There are many works on the use of HAP as drug carriers, likewise cellulose in the literature; however, comprehensive study on their combination as drug carriers are not well characterized, which indicates the need for a careful study to corroborate and explore such research areas for further comprehensive in vivo studies.

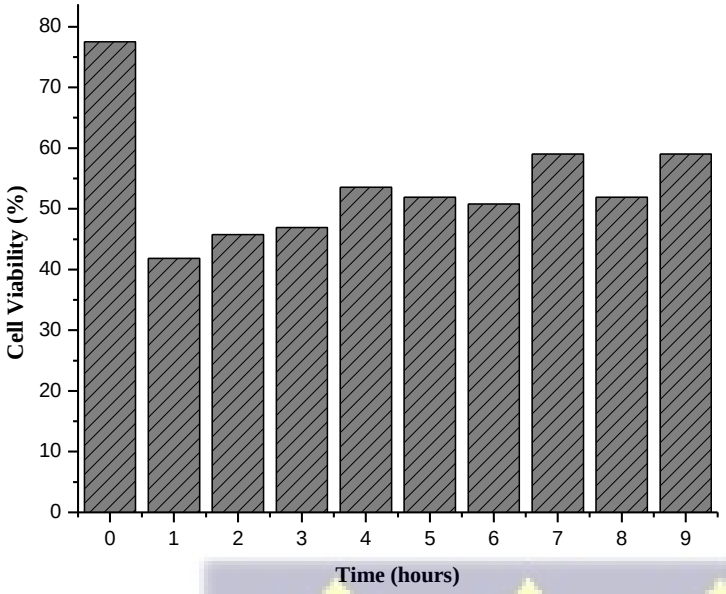

Figure 4.14: Cell viability of 2.0 mg CNC/HAP composite using MTT assay.

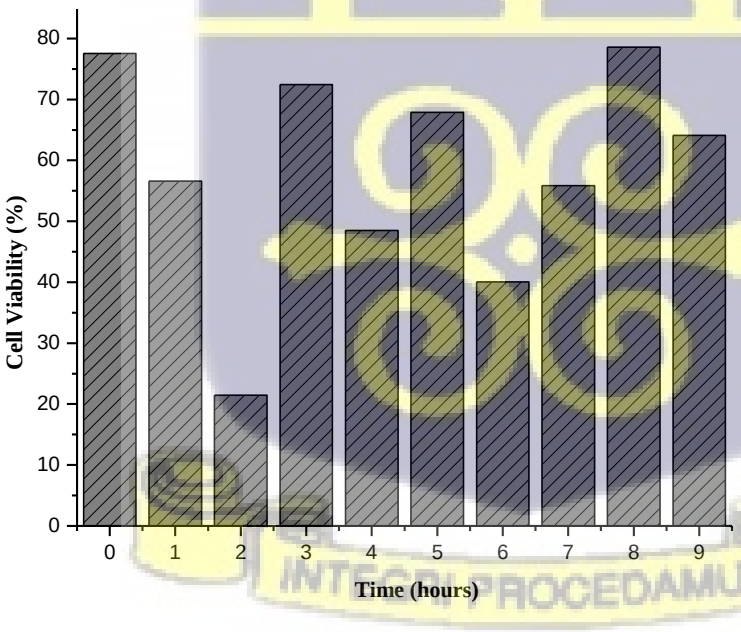

Figure 4.15: Cell viability of HAP using MTT assay.

CHAPTER FIVE

5.0 Summary

This study was conducted to synthesize biocomposites from hydroxyapatite and cellulose nanocrystals and examine their chemical and functional properties. The properties of the individual materials were compared with the synthesized composites. Composites with hydroxyapatite as base material were loaded with a model drug (curcumin) and the release of the drug was studied in acidic and neutral pH with hydroxyapatite as control. Drug release in pH ≈ 6.2 released a higher percentage of drug as compared to composites in pH ≈ 7.4. The drug release kinetics were studied and fitted to Higuchi and Korsmeyer-Peppas models. The cubic order polynomial suggested that three factors (concentration gradient of the drug, diffusion distance of the drug from the composite to the release environment and the surface area of the composite) could contribute to the rate of drug release from the composites. Loaded composites (2.0 mg CNC/HAP) were tested on MDA-MB-231 cells with loaded HAP as control. Cell viability results indicated that combining HAP and cellulose serves as a better option for a drug carrier to MDA-MB-231 cells than HAP only.

5.1 Conclusion

Hydroxyapatite has gained interest in biomedical engineering, particularly drug delivery applications due to its tunable properties and ability to modify it for specific biomedical applications. From the study the following can be concluded

1. Composites were synthesized from hydroxyapatite and cellulose. This was confirmed from the characterization of the composites from FTIR and XRD data.

2. The model drug, curcumin was loaded onto the composites for 22 hours. The loaded composites and the control did not show any significant difference. The average entrapment efficiency of drug loaded was about 85%.
3. The release properties of the composites were studied *in vitro* in 50% DMSO in acidic medium (pH ≈ 6.2) and neutral medium (pH ≈ 7.4) for 6 hours. The release percentages of 0.5 mg CNC/HAP, 1.0 mg CNC/HAP, 1.5 mg CNC/HAP, 2.0 mg CNC/HAP composites and HAP after 6 hours were 32.87± 1.20%, 29.89± 4.87%, 33.78± 2.73%, 32.14± 5.14% and 35.36± 0.52% respectively in pH ≈ 6.2. In pH ≈ 7.4, the composites released 18.99± 0.23%, 16.52± 0.83%, 23.32±0.38%, 19.60± 0.16% and 27.95±2.38% respectively. Composites in pH ≈ 7.4 had a sustained release of the drug with 1.0 mg CNC/HAP composite showing the most sustained release. One-way analysis of variance (ANOVA) showed that there was no significant difference in drug release between the composites and the control in pH ≈ 6.2. However, the release was statistically significant in pH ≈ 7.4 and across groups. Tukey post hoc test was further carried out and it was realized that there was significant difference in the drug release between the composites in pH ≈ 7.4 and the control but no significant difference was seen when a pairwise comparison was performed between the composites. The Tukey test also showed that there was significant difference between the means across the groups for all the composites. However, there was no difference in the means of control (HAP).
4. After fitting the drug release data to release models, it was observed that all composites and the control in both medium (pH ≈ 6.2 and pH ≈ 7.4) are best described by the Korsmeyer-Peppas model. The diffusion coefficient factor from Kormeyer-Peppas model showed that the drug release is Fickian diffusion. The cubic degree polynomial revealed

that there were three factors at play that affected the drug release from the composites. This could be concentration of the drug, diffusion distance and the surface area of the composites.

5. Cell viability studies showed that modified composites (2.0 mg CNC/HAP) released the drug (curcumin) at a controlled rate as compared to HAP (control). The modified composites (2.0 mg CNC/HAP) inhibited cell growth at all time points during the nine hours of drug release. The combination of HAP and 2. 0 mg cellulose serves as a better drug delivery system than HAP only.

5.2 Recommendation

It is recommended that more characterizations are conducted on the resulting composites to get more information about the surface charges, pore diameter among others to elucidate the three factors that are suggested by the cubic degree polynomial. It is also recommended that animal models are employed to assess the systemic effect of the loaded composites. Future directions should also focus on increasing the drug release time and the ratio of hydroxyapatite and cellulose nanocrystal in composite formation to examine the drug release based on the resulting composites.

6.0 References

Abidi, N., Hequet, E., Cabrales, L., Gannaway, J., Wilkins, T., & Wells, L. W. (2008). Evaluating cell wall structure and composition of developing cotton fibers using fourier transform infrared spectroscopy and thermogravimetric analysis. *Journal of Applied Polymer Science*, *107*(1), 476–486. https://doi.org/10.1002/app.27100

Abo-Elseoud, W. S., Hassan, M. L., Sabaa, M. W., Basha, M., Hassan, E. A., & Fadel, S. M. (2018). Chitosan nanoparticles/cellulose nanocrystals nanocomposites as a carrier system for the controlled release of repaglinide. *International Journal of Biological Macromolecules*, *111*, 604–613. https://doi.org/10.1016/j.ijbiomac.2018.01.044

Åhlén, M., Tummala, G. K., & Mihranyan, A. (2018). Nanoparticle-loaded hydrogels as a pathway for enzyme-triggered drug release in ophthalmic applications. *International Journal of Pharmaceutics*, *536*(1), 73–81. https://doi.org/10.1016/j.ijpharm.2017.11.053

Åkerholm, M., Hinterstoisser, B., & Salmén, L. (2004). Characterization of the crystalline structure of cellulose using static and dynamic FT-IR spectroscopy. *Carbohydrate Research*, *339*(3), 569–578. https://doi.org/10.1016/j.carres.2003.11.012

Alkilani, A. Z., McCrudden, M. T. C., & Donnelly, R. F. (2015). Transdermal drug delivery: Innovative pharmaceutical developments based on disruption of the barrier properties of the stratum corneum. *Pharmaceutics*, Vol. 7, pp. 438–470. https://doi.org/10.3390/pharmaceutics7040438

Amandeep Kaur, N. S. and S. L. H. (2013). Design and Development of Ketoprofen Pharmacosomes for. *Pharmacophore,An International Research Journalesearch Journal*,

4(4), 111–119.

Andrés, N. C., Sieben, J. M., Baldini, M., Rodríguez, C. H., Famiglietti, Á., & Messina, P. V. (2018). Electroactive Mg2+-Hydroxyapatite Nanostructured Networks against Drug-Resistant Bone Infection Strains. *ACS Applied Materials and Interfaces*, *10*(23), 19534–19544. https://doi.org/10.1021/acsami.8b06055

Asimeng, B. O., Tiburu, E. K., Effah Kaufmann, E., Paemka, L., Hayford, C. F., Essien-Baidoo, S., … Anani, P. A. (2019). Electrochemical evaluation of ion substituted-hydroxyapatite on HeLa cells plasma membrane potential. *Cogent Engineering*, *6*(1). https://doi.org/10.1080/23311916.2019.1614756

Attia, M. F., Anton, N., Wallyn, J., Omran, Z., & Vandamme, T. F. (2019). An overview of active and passive targeting strategies to improve the nanocarriers efficiency to tumour sites. *Journal of Pharmacy and Pharmacology*, Vol. 71, pp. 1185–1198. https://doi.org/10.1111/jphp.13098

Banerjee, M., Saraswatula, S., Williams, A., & Brettmann, B. (2020). Effect of purification methods on commercially available cellulose nanocrystal properties and TEMPO oxidation. *Processes*, *8*(6), 698. https://doi.org/10.3390/PR8060698

Beck-Candanedo, S., Roman, M., & Gray, D. G. (2005). Effect of reaction conditions on the properties and behavior of wood cellulose nanocrystal suspensions. *Biomacromolecules*, *6*(2), 1048–1054. https://doi.org/10.1021/bm049300p

Berzina-Cimdina, L., & Borodajenko, N. (2012). Research of Calcium Phosphates Using Fourier Transform Infrared Spectroscopy. In *Infrared Spectroscopy - Materials Science, Engineering*

and Technology. https://doi.org/10.5772/36942

Brinchi, L., Cotana, F., Fortunati, E., & Kenny, J. M. (2013). Production of nanocrystalline cellulose from lignocellulosic biomass: Technology and applications. *Carbohydrate Polymers*, Vol. 94, pp. 154–169. https://doi.org/10.1016/j.carbpol.2013.01.033

Bulysheva, A. A., Sori, N., & Francis, M. P. (2018). Direct crystal formation from micronized bone and lactic acid: The writing on the wall for calcium-containing crystal pathogenesis in osteoarthritis? *PLoS ONE*, *13*(11). https://doi.org/10.1371/journal.pone.0202373

Bunaciu, A. A., Udriştioiu, E. gabriela, & Aboul-Enein, H. Y. (2015). X-Ray Diffraction: Instrumentation and Applications. *Critical Reviews in Analytical Chemistry*, Vol. 45, pp. 289–299. https://doi.org/10.1080/10408347.2014.949616

Cazalbou, S., Eichert, D., Ranz, X., Drouet, C., Combes, C., Harmand, M. F., & Rey, C. (2005). Ion exchanges in apatites for biomedical application. *Journal of Materials Science: Materials in Medicine*, *16*(5), 405–409. https://doi.org/10.1007/s10856-005-6979-2

Chakrabarty, A., & Teramoto, Y. (2018). Recent advances in nanocellulose composites with polymers: A guide for choosing partners and how to incorporate them. *Polymers*, Vol. 10. https://doi.org/10.3390/polym10050517

Chen, S., Shi, Y., Luo, Y., & Ma, J. (2019). Layer-by-layer coated porous 3D printed hydroxyapatite composite scaffolds for controlled drug delivery. *Colloids and Surfaces B: Biointerfaces*, *179*, 121–127. https://doi.org/10.1016/j.colsurfb.2019.03.063

Chen, X., Wang, Q., Shen, J., Pan, H., & Wu, T. (2007). Adsorption of leucine-rich amelogenin protein on hydroxyapatite (001) surface through -COO- claws. *Journal of Physical Chemistry*

C, *111*(3), 1284–1290. https://doi.org/10.1021/jp0646630

Dai, R., Wang, Z., Samanipour, R., Koo, K. I., & Kim, K. (2016). Adipose-Derived Stem Cells for Tissue Engineering and Regenerative Medicine Applications. *Stem Cells International*, *2016*. https://doi.org/10.1155/2016/6737345

Dias, A. P., da Silva Santos, S., da Silva, J. V., Parise-Filho, R., Igne Ferreira, E., Seoud, O. El, & Giarolla, J. (2020). Dendrimers in the context of nanomedicine. *International Journal of Pharmaceutics*, Vol. 573. https://doi.org/10.1016/j.ijpharm.2019.118814

El Khouri, A., Zegzouti, A., Elaatmani, M., & Capitelli, F. (2019). Bismuth-substituted hydroxyapatite ceramics synthesis: Morphological, structural, vibrational and dielectric properties. *Inorganic Chemistry Communications*, *110*. https://doi.org/10.1016/j.inoche.2019.107568

Elazzouzi-Hafraoui, S., Nishiyama, Y., Putaux, J. L., Heux, L., Dubreuil, F., & Rochas, C. (2008). The shape and size distribution of crystalline nanoparticles prepared by acid hydrolysis of native cellulose. *Biomacromolecules*, *9*(1), 57–65. https://doi.org/10.1021/bm700769p

Eyley, S., & Thielemans, W. (2014). Surface modification of cellulose nanocrystals. *Nanoscale*, *6*(14), 7764–7779. https://doi.org/10.1039/c4nr01756k

Fan, M., Dai, D., & Huang, B. (2012). Fourier Transform Infrared Spectroscopy for Natural Fibres. In *Fourier Transform - Materials Analysis*. https://doi.org/10.5772/35482

Farnia, F., Fan, W., Dory, Y., & Zhao, Y. (2019). Making Nanocomposites of Hydrophilic and Hydrophobic Polymers Using Gas-Responsive Cellulose Nanocrystals. *Macromolecular Rapid Communications*, *40*(12). https://doi.org/10.1002/marc.201900114

Ferrari, R., Sponchioni, M., Morbidelli, M., & Moscatelli, D. (2018). Polymer nanoparticles for the intravenous delivery of anticancer drugs: The checkpoints on the road from the synthesis to clinical translation. *Nanoscale*, Vol. 10, pp. 22701–22719. https://doi.org/10.1039/c8nr05933k

Gasser, P., Haikel, Y., Voegel, J. C., & Gramain, P. (1994). Surface reactions of hydroxyapatite in the presence of fluoride ions 2. Effects of calcium and phosphate in saturated solutions. *Colloids and Surfaces A: Physicochemical and Engineering Aspects*, *88*(2–3), 157–168. https://doi.org/10.1016/0927-7757(94)02783-8

George, J., & Siddaramaiah. (2012). High performance edible nanocomposite films containing bacterial cellulose nanocrystals. *Carbohydrate Polymers*, *87*(3), 2031–2037. https://doi.org/10.1016/j.carbpol.2011.10.019

Ghiasi, B., Sefidbakht, Y., & Rezaei, M. (2019). Hydroxyapatite for biomedicine and drug delivery. In *Advanced Structured Materials* (Vol. 104, pp. 85–120). https://doi.org/10.1007/978-3-030-10834-2_4

Gopinath, A., & Wilson, M. (2020). Factors affecting drug absorption and distribution. *Anaesthesia and Intensive Care Medicine*, Vol. 21, pp. 223–228. https://doi.org/10.1016/j.mpaic.2020.02.003

Gozalian, A., Behnamghader, A., Daliri, M., & Moshkforoush, A. (2011). Synthesis and thermal behavior of Mg-doped calcium phosphate nanopowders via the sol gel method. *Scientia Iranica*, *18*(6), 1614–1622. https://doi.org/10.1016/j.scient.2011.11.014

Gupta, R. D., & Raghav, N. (2020). Nano-crystalline cellulose: Preparation, modification and

usage as sustained release drug delivery excipient for some non-steroidal anti-inflammatory drugs. *International Journal of Biological Macromolecules*, *147*, 921–930. https://doi.org/10.1016/j.ijbiomac.2019.10.057

Habibi, Y., Lucia, L. A., & Rojas, O. J. (2010). Cellulose nanocrystals: Chemistry, self-assembly, and applications. *Chemical Reviews*, *110*(6), 3479–3500. https://doi.org/10.1021/cr900339w

Haider, A., Haider, S., Han, S. S., & Kang, I. K. (2017). Recent advances in the synthesis, functionalization and biomedical applications of hydroxyapatite: a review. *RSC Advances*, Vol. 7, pp. 7442–7458. https://doi.org/10.1039/c6ra26124h

Hare, J. I., Lammers, T., Ashford, M. B., Puri, S., Storm, G., & Barry, S. T. (2017). Challenges and strategies in anti-cancer nanomedicine development: An industry perspective. *Advanced Drug Delivery Reviews*, Vol. 108, pp. 25–38. https://doi.org/10.1016/j.addr.2016.04.025

He, H., Liang, Q., Shin, M. C., Lee, K., Gong, J., Ye, J., Yang, V. (2013). Significance and strategies in developing delivery systems for bio-macromolecular drugs. *Frontiers of Chemical Science and Engineering*, Vol. 7, pp. 496–507. https://doi.org/10.1007/s11705-013-1362-1

He, H., Lu, Y., Qi, J., Zhu, Q., Chen, Z., & Wu, W. (2019). Adapting liposomes for oral drug delivery. *Acta Pharmaceutica Sinica B*, Vol. 9, pp. 36–48. https://doi.org/10.1016/j.apsb.2018.06.005

Heath, J. R. (2015). Nanotechnologies for biomedical science and translational medicine. *Proceedings of the National Academy of Sciences of the United States of America*, *112*(47), 14436–14443. https://doi.org/10.1073/pnas.1515202112

Hedaya, M. A. (2012). Extravascular routes of drug administration. In *Basic Pharmacokinetics* (p. 595).

Hickey, R. J., Modulevsky, D. J., Cuerrier, C. M., & Pelling, A. E. (2018). Customizing the Shape and Microenvironment Biochemistry of Biocompatible Macroscopic Plant-Derived Cellulose Scaffolds. *ACS Biomaterials Science and Engineering*, *4*(11), 3726–3736. https://doi.org/10.1021/acsbiomaterials.8b00178

Huang, X., & Brazel, C. S. (2001). On the importance and mechanisms of burst release in matrix-controlled drug delivery systems. *Journal of Controlled Release*, *73*(2–3), 121–136. https://doi.org/10.1016/S0168-3659(01)00248-6

Huang, Z. Y., Li, X. X., Liu, Z. J., He, L. M., & Tan, X. C. (2015). Morphology effect on the kinetic parameters and surface thermodynamic properties of ag3po4 micro-/nanocrystals. *Journal of Nanomaterials*, *2015*. https://doi.org/10.1155/2015/743121

Jackson, J. K., Letchford, K., Wasserman, B. Z., Ye, L., Hamad, W. Y., & Burt, H. M. (2011). The use of nanocrystalline cellulose for the binding and controlled release of drugs. *International Journal of Nanomedicine*, *6*, 321–330. https://doi.org/10.2147/ijn.s16749

Jain, A. K., Sahu, P. K., Mohan, P., & Jain, S. J. (2016). Ion Exchange Resins- Pharmaceutical and Clinical Applications. *Asian Journal of Biomaterial Research*, *2*(2), 51–61.

Jain, K. K. (2020). An Overview of Drug Delivery Systems. In *Methods in Molecular Biology* (Vol. 2059, pp. 1–54). https://doi.org/10.1007/978-1-4939-9798-5_1

Jorfi, M., & Foster, E. J. (2015). Recent advances in nanocellulose for biomedical applications. *Journal of Applied Polymer Science*, Vol. 132. https://doi.org/10.1002/app.41719

Jurásek, B., Bartůněk, V., Huber, Š., & Kuchař, M. (2019). X-Ray powder diffraction – A non-destructive and versatile approach for the identification of new psychoactive substances. *Talanta*, *195*, 414–418. https://doi.org/10.1016/j.talanta.2018.11.063

Kallel, F., Bettaieb, F., Khiari, R., García, A., Bras, J., & Chaabouni, S. E. (2016). Isolation and structural characterization of cellulose nanocrystals extracted from garlic straw residues. *Industrial Crops and Products*, *87*, 287–296. https://doi.org/10.1016/j.indcrop.2016.04.060

Kang, H., Liu, R., & Huang, Y. (2015). Graft modification of cellulose: Methods, properties and applications. *Polymer*, Vol. 70, pp. A1–A16. https://doi.org/10.1016/j.polymer.2015.05.041

Kargarzadeh, H., Mariano, M., Gopakumar, D., Ahmad, I., Thomas, S., Dufresne, A., … Lin, N. (2018). Advances in cellulose nanomaterials. *Cellulose*, Vol. 25, pp. 2151–2189. https://doi.org/10.1007/s10570-018-1723-5

Kenawy, E. R., Azaam, M. M., Afzal, M., Khatoon, A., Ansari, M. T., & Hasnain, M. S. (2020). Pharmaceutical application of cellulose derivatives. In *Tailor-Made Polysaccharides in Biomedical Applications* (pp. 305–328). https://doi.org/10.1016/b978-0-12-821344-5.00013-8

Kok-Yong, S., & Lawrence, L. (2015). Drug Distribution and Drug Elimination. In *Basic Pharmacokinetic Concepts and Some Clinical Applications*. https://doi.org/10.5772/59929

Kumar, S., & Gupta, S. K. (2012). Natural polymers, gums and mucilages as excipients in drug delivery. *Polimery W Medycynie*, Vol. 42, pp. 191–197.

Laaksonen, T., Ahonen, P., Johans, C., & Kontturi, K. (2006). Stability and electrostatics of mercaptoundecanoic acid-capped gold nanoparticles with varying counterion size.

ChemPhysChem, *7*(10), 2143–2149. https://doi.org/10.1002/cphc.200600307

Lam, E., Male, K. B., Chong, J. H., Leung, A. C. W., & Luong, J. H. T. (2012). Applications of functionalized and nanoparticle-modified nanocrystalline cellulose. *Trends in Biotechnology*, Vol. 30, pp. 283–290. https://doi.org/10.1016/j.tibtech.2012.02.001

Lee, K. Y., Blaker, J. J., & Bismarck, A. (2009). Surface functionalisation of bacterial cellulose as the route to produce green polylactide nanocomposites with improved properties. *Composites Science and Technology*, *69*(15–16), 2724–2733. https://doi.org/10.1016/j.compscitech.2009.08.016

Lee, P. I., & Li, J. X. (2010). Evolution of oral controlled release dosage forms. In *Oral Controlled Release Formulation Design and Drug Delivery: Theory to Practice* (pp. 21–31). https://doi.org/10.1002/9780470640487.ch2

Lei, W., Sun, C., Jiang, T., Gao, Y., Yang, Y., Zhao, Q., & Wang, S. (2019). Polydopamine-coated mesoporous silica nanoparticles for multi-responsive drug delivery and combined chemo-photothermal therapy. *Materials Science and Engineering C*, *105*. https://doi.org/10.1016/j.msec.2019.110103

Li, D., & Kaner, R. B. (2006). Shape and aggregation control of nanoparticles: Not shaken, not stirred. *Journal of the American Chemical Society*, *128*(3), 968–975. https://doi.org/10.1021/ja056609n

Luque, P. A., Cervantes, D., Gomez-Gutierrez, C. M., Carrillo-Castillo, A., Mota-Gonzalez, M. L., Vilchis-Nestor, A. R., & Olivas, A. (2017). Synthesis and characterization of terbium doped hydroxyapatite at different percentages by weight. *Digest Journal of Nanomaterials*

and Biostructures, *12*(1), 135–139.

Meesorn, W., Shirole, A., Vanhecke, D., De Espinosa, L. M., & Weder, C. (2017). A Simple and Versatile Strategy to Improve the Mechanical Properties of Polymer Nanocomposites with Cellulose Nanocrystals. *Macromolecules*, *50*(6), 2364–2374. https://doi.org/10.1021/acs.macromol.6b02629

Mizushima, Y., Ikoma, T., Tanaka, J., Hoshi, K., Ishihara, T., Ogawa, Y., & Ueno, A. (2006). Injectable porous hydroxyapatite microparticles as a new carrier for protein and lipophilic drugs. *Journal of Controlled Release*, *110*(2), 260–265. https://doi.org/10.1016/j.jconrel.2005.09.051

Modulevsky, D. J., Cuerrier, C. M., & Pelling, A. E. (2016). Biocompatibility of Subcutaneously Implanted Plant-Derived Cellulose Biomaterials. *PLoS ONE*, *11*(6). https://doi.org/10.1371/journal.pone.0157894

Mohd Pu'ad, N. A. S., Koshy, P., Abdullah, H. Z., Idris, M. I., & Lee, T. C. (2019). Syntheses of hydroxyapatite from natural sources. *Heliyon*, Vol. 5. https://doi.org/10.1016/j.heliyon.2019.e01588

Mollazadeh, S., Mackiewicz, M., & Yazdimamaghani, M. (2021). Recent advances in the redox-responsive drug delivery nanoplatforms: A chemical structure and physical property perspective. *Materials Science and Engineering C*, Vol. 118. https://doi.org/10.1016/j.msec.2020.111536

Moniri, M., Moghaddam, A. B., Azizi, S., Rahim, R. A., Ariff, A. Bin, Saad, W. Z., … Mohamad, R. (2017). Production and status of bacterial cellulose in biomedical engineering.

Nanomaterials, Vol. 7. https://doi.org/10.3390/nano7090257

Montanari, S., Roumani, M., Heux, L., & Vignon, M. R. (2005). Topochemistry of carboxylated cellulose nanocrystals resulting from TEMPO-mediated oxidation. *Macromolecules*, *38*(5), 1665–1671. https://doi.org/10.1021/ma048396c

Moon, R. J., Martini, A., Nairn, J., Simonsen, J., & Youngblood, J. (2011). Cellulose nanomaterials review: Structure, properties and nanocomposites. *Chemical Society Reviews*, *40*(7), 3941–3994. https://doi.org/10.1039/c0cs00108b

Nandiyanto, A. B. D., Oktiani, R., & Ragadhita, R. (2019). How to read and interpret ftir spectroscope of organic material. *Indonesian Journal of Science and Technology*, *4*(1), 97–118. https://doi.org/10.17509/ijost.v4i1.15806

Parhiz, H., Khoshnejad, M., Myerson, J. W., Hood, E., Patel, P. N., Brenner, J. S., & Muzykantov, V. R. (2018). Unintended effects of drug carriers: Big issues of small particles. *Advanced Drug Delivery Reviews*, Vol. 130, pp. 90–112. https://doi.org/10.1016/j.addr.2018.06.023

Park, K. (2014). Controlled drug delivery systems: Past forward and future back. *Journal of Controlled Release*, Vol. 190, pp. 3–8. https://doi.org/10.1016/j.jconrel.2014.03.054

Pasut, G. (2019). Grand Challenges in Nano-Based Drug Delivery. *Frontiers in Medical Technology*, *1*. https://doi.org/10.3389/fmedt.2019.00001

Patel, J., Basu, B., Dharamsi, A., Garala, K., & Raval, M. (2011). Solubility of aceclofenac in polyamidoamine dendrimer solutions. *International Journal of Pharmaceutical Investigation*, *1*(3), 135. https://doi.org/10.4103/2230-973x.85962

Portioli, C., Bovi, M., Benati, D., Donini, M., Perduca, M., Romeo, A., Bentivoglio, M. (2017).

Novel functionalization strategies of polymeric nanoparticles as carriers for brain medications. *Journal of Biomedical Materials Research - Part A*, *105*(3), 847–858. https://doi.org/10.1002/jbm.a.35961

Prasanna, A. P. S., & Venkatasubbu, G. D. (2018). Sustained release of amoxicillin from hydroxyapatite nanocomposite for bone infections. *Progress in Biomaterials*, *7*(4), 289–296. https://doi.org/10.1007/s40204-018-0103-4

Predoi, D., Groza, A., Iconaru, S. L., Predoi, G., Barbuceanu, F., Guegan, R., Cimpeanu, C. (2018). Properties of basil and lavender essential oils adsorbed on the surface of hydroxyapatite. *Materials*, *11*(5). https://doi.org/10.3390/ma11050652

Putro, J. N., Ismadji, S., Gunarto, C., Soetaredjo, F. E., & Ju, Y. H. (2019). Effect of natural and synthetic surfactants on polysaccharide nanoparticles: Hydrophobic drug loading, release, and cytotoxic studies. *Colloids and Surfaces A: Physicochemical and Engineering Aspects*, *578*. https://doi.org/10.1016/j.colsurfa.2019.123618

Raghav, N., Mor, N., Gupta, R. D., Kaur, R., Sharma, M. R., & Arya, P. (2020). Some cetyltrimethylammonium bromide modified polysaccharide supports as sustained release systems for curcumin. *International Journal of Biological Macromolecules*, *154*, 361–370. https://doi.org/10.1016/j.ijbiomac.2020.02.317

Riaz, M., Zia, R., Ijaz, A., Hussain, T., Mohsin, M., & Malik, A. (2018). Synthesis of monophasic Ag doped hydroxyapatite and evaluation of antibacterial activity. *Materials Science and Engineering C*, *90*, 308–313. https://doi.org/10.1016/j.msec.2018.04.076

Rimmington, F. (2020). Pharmacokinetics and pharmacodynamics. *Southern African Journal of*

Anaesthesia and Analgesia, *26*(6), S153–S156. https://doi.org/10.36303/SAJAA.2020.26.6.S3.2562

Roman, M., Dong, S., Hirani, A., & Lee, Y. W. (2009). Cellulose nanocrystals for drug delivery. *ACS Symposium Series*, *1017*, 81–91. https://doi.org/10.1021/bk-2009-1017.ch004

Sadat-Shojai, M., Khorasani, M. T., Dinpanah-Khoshdargi, E., & Jamshidi, A. (2013). Synthesis methods for nanosized hydroxyapatite with diverse structures. *Acta Biomaterialia*, Vol. 9, pp. 7591–7621. https://doi.org/10.1016/j.actbio.2013.04.012

Safdari, F., Carreau, P. J., Heuzey, M. C., Kamal, M. R., & Sain, M. M. (2017). Enhanced properties of poly(ethylene oxide)/cellulose nanofiber biocomposites. *Cellulose*, *24*(2), 755–767. https://doi.org/10.1007/s10570-016-1137-1

Sanchez, C., Julián, B., Belleville, P., & Popall, M. (2005). Applications of hybrid organic-inorganic nanocomposites. *Journal of Materials Chemistry*, *15*(35–36), 3559–3592. https://doi.org/10.1039/b509097k

Saravanakumar, K., Swapna, P., Nagaveni, P., Vani, P., & Pujitha, K. (2015). Transdermal drug delivery system: A review. *Journal of Global Trends in Pharmaceutical Sciences*, Vol. 6, pp. 2485–2490. https://doi.org/10.46624/ajptr.2020.v10.i2.004

Schwanninger, M., Rodrigues, J. C., Pereira, H., & Hinterstoisser, B. (2004). Effects of short-time vibratory ball milling on the shape of FT-IR spectra of wood and cellulose. *Vibrational Spectroscopy*, *36*(1), 23–40. https://doi.org/10.1016/j.vibspec.2004.02.003

Senior, J., Radomsky, M., & Group, F. (2000). *Sustained-Release Injectable Products Edited by*.

Setiawan, A., Widiyastuti, W., Winardi, S., & Nugroho, A. (2017). Sintesis biomaterial

hydroxyapatite dengan proses flame spray pyrolysis disertai penambahan aditif organik. *Reaktor*, *16*(4), 189. https://doi.org/10.14710/reaktor.16.4.189-198

Shankaran, D. R. (2018). Cellulose Nanocrystals for Health Care Applications. In *Applications of Nanomaterials*. https://doi.org/10.1016/b978-0-08-101971-9.00015-6

Sharma, A., & Kakkar, A. (2015). Designing dendrimer and miktoarm polymer based multi-tasking nanocarriers for efficient medical therapy. *Molecules*, Vol. 20, pp. 16987–17015. https://doi.org/10.3390/molecules200916987

Sharma, S., Aiswarya, T. T., Mirza, I., & Saha, S. (2020). Biocompatible Polymers and its Applications. In *Reference Module in Materials Science and Materials Engineering*. https://doi.org/10.1016/b978-0-12-820352-1.00044-4

Shi, Z., Zang, S., Jiang, F., Huang, L., Lu, D., Ma, Y., & Yang, G. (2012). In situ nano-assembly of bacterial cellulose-polyaniline composites. *RSC Advances*, *2*(3), 1040–1046. https://doi.org/10.1039/c1ra00719j

Shi, Z., Zhou, Y., Fan, T., Lin, Y., Zhang, H., & Mei, L. (2020). Inorganic nano-carriers based smart drug delivery systems for tumor therapy. *Smart Materials in Medicine*, Vol. 1, pp. 32–47. https://doi.org/10.1016/j.smaim.2020.05.002

Skwarek, E., & Janusz, W. (2019). Adsorption of Ba 2+ ions at the hydroxyapatite/NaCl solution interface. *Adsorption*, *25*(3), 279–288. https://doi.org/10.1007/s10450-018-00005-1

Smičiklas, I., Onjia, A., Marković, J., & Raičević, S. (2005). Comparison of Hydroxyapatite Sorption Properties towards Cadmium, Lead, Zinc and Strontium Ions. *Materials Science Forum*, *494*, 405–410. https://doi.org/10.4028/www.scientific.net/msf.494.405

Sperling, R. A., & Parak, W. J. (2010). Surface modification, functionalization and bioconjugation of colloidal Inorganic nanoparticles. *Philosophical Transactions of the Royal Society A: Mathematical, Physical and Engineering Sciences*, Vol. 368, pp. 1333–1383. https://doi.org/10.1098/rsta.2009.0273

Sugiyama, S., Ichii, T., Fujisawa, M., Kawashiro, K., Tomida, T., Shigemoto, N., & Hayashi, H. (2003). Heavy metal immobilization in aqueous solution using calcium phosphate and calcium hydrogen phosphates. *Journal of Colloid and Interface Science*, *259*(2), 408–410. https://doi.org/10.1016/S0021-9797(02)00211-4

Terpáková, E., Kidalová, L., Eštoková, A., Čigášová, J., & Števulová, N. (2012). Chemical modification of hemp shives and their characterization. *Procedia Engineering*, *42*, 931–941. https://doi.org/10.1016/j.proeng.2012.07.486

Thürmann, P. A. (2020). Pharmacodynamics and pharmacokinetics in older adults. *Current Opinion in Anaesthesiology*, Vol. 33, pp. 109–113. https://doi.org/10.1097/ACO.0000000000000814

Tiwari, G., Tiwari, R., Bannerjee, S., Bhati, L., Pandey, S., Pandey, P., & Sriwastawa, B. (2012). Drug delivery systems: An updated review. *International Journal of Pharmaceutical Investigation*, *2*(1), 2. https://doi.org/10.4103/2230-973x.96920

Tovar-Carrillo, K. L., Saucedo-Acuña, R. A., Ríos-Arana, J., Tamayo, G., Guzmán-Gastellum, D. A., Díaz-Torres, B. A., Cuevas-González, J. C. (2020). Synthesis, Characterization, and in Vitro and in Vivo Evaluations of Cellulose Hydrogels Enriched with Larrea tridentata for Regenerative Applications. *BioMed Research International*, *2020*. https://doi.org/10.1155/2020/1425402

Varma, H. K., & Babu, S. S. (2005). Synthesis of calcium phosphate bioceramics by citrate gel pyrolysis method. *Ceramics International*, *31*(1), 109–114. https://doi.org/10.1016/j.ceramint.2004.03.041

Versypt, A. F. (2015). *Modeling of controlled-release drug delivery from autocatalytically degrading polymer microspheres*. 1–256.

Wang, Q., Zhao, X., & Zhu, J. Y. (2014). Kinetics of strong acid hydrolysis of a bleached kraft pulp for producing cellulose nanocrystals (CNCs). *Industrial and Engineering Chemistry Research*, *53*(27), 11007–11014. https://doi.org/10.1021/ie501672m

Wang, Y., Li, H., Wang, L., Han, J., Yang, Y., Fu, T., Li, J. (2021). Mucoadhesive nanocrystal-in-microspheres with high drug loading capacity for bioavailability enhancement of silybin. *Colloids and Surfaces B: Biointerfaces*, *198*. https://doi.org/10.1016/j.colsurfb.2020.111461

Wei, G., & Ma, P. X. (2004). Structure and properties of nano-hydroxyapatite/polymer composite scaffolds for bone tissue engineering. *Biomaterials*, *25*(19), 4749–4757. https://doi.org/10.1016/j.biomaterials.2003.12.005

Williams, D. F. (2014). There is no such thing as a biocompatible material. *Biomaterials*, *35*(38), 10009–10014. https://doi.org/10.1016/j.biomaterials.2014.08.035

Wilson, B., Samanta, M. K., Santhi, K., Kumar, K. P. S., Ramasamy, M., & Suresh, B. (2010). Chitosan nanoparticles as a new delivery system for the anti-Alzheimer drug tacrine. *Nanomedicine: Nanotechnology, Biology, and Medicine*, *6*(1), 144–152. https://doi.org/10.1016/j.nano.2009.04.001

Wohlhauser, S., Delepierre, G., Labet, M., Morandi, G., Thielemans, W., Weder, C., & Zoppe, J.

O. (2018). Grafting Polymers from Cellulose Nanocrystals: Synthesis, Properties, and Applications. *Macromolecules*, Vol. 51, pp. 6157–6189. https://doi.org/10.1021/acs.macromol.8b00733

Wu, W., Huang, F., Pan, S., Mu, W., Meng, X., Yang, H., Deng, Y. (2015). Thermo-responsive and fluorescent cellulose nanocrystals grafted with polymer brushes. *Journal of Materials Chemistry A*, *3*(5), 1995–2005. https://doi.org/10.1039/c4ta04761c

Yang, R., Wei, T., Goldberg, H., Wang, W., Cullion, K., & Kohane, D. S. (2017). Getting Drugs Across Biological Barriers. *Advanced Materials*, Vol. 29. https://doi.org/10.1002/adma.201606596

Yokota, T., Nakano, K., Nagaya, M., Honda, M., Nagashima, H., & Aizawa, M. (2018). In vivo evaluation of porous hydroxyapatite ceramics including bone minerals using pig model. *Materials Technology*, *33*(10), 689–697. https://doi.org/10.1080/10667857.2018.1495392

Yoo, J., Park, C., Yi, G., Lee, D., & Koo, H. (2019). Active targeting strategies using biological ligands for nanoparticle drug delivery systems. *Cancers*, *11*(5). https://doi.org/10.3390/cancers11050640

Yusufoglu, Y., & Akinc, M. (2008). Effect of pH on the carbonate incorporation into the hydroxyapatite prepared by an oxidative decomposition of calcium-EDTA chelate. *Journal of the American Ceramic Society*, *91*(1), 77–82. https://doi.org/10.1111/j.1551-2916.2007.02092.x

Zhong, C. (2020). Industrial-Scale Production and Applications of Bacterial Cellulose. *Frontiers in Bioengineering and Biotechnology*, Vol. 8. https://doi.org/10.3389/fbioe.2020.605374

Zhu, Y., Liu, J., Zhu, W., Cai, Y., Kundu, S. C., & Yao, J. (2015). Surface modification of hydroxyapatite microspheres for the sustained release of vitamin C. *Materials Technology*, *30*, 223–228. https://doi.org/10.1179/17535557B15Y.000000007

Zubik, K., Singhsa, P., Wang, Y., Manuspiya, H., & Narain, R. (2017). Thermo-responsive poly(N-isopropylacrylamide)-cellulose nanocrystals hybrid hydrogels for wound dressing. *Polymers*, *9*(4). https://doi.org/10.3390/polym9040119

7.0 Appendices

Supplementary tables and figures

Table S1: Percentage drug release data in pH ≈ 6.2 from first experiment

Time/hrs	HAP Only	0.5 mg CNC/HAP	1.0 mg CNC/HAP	1.5 mg CNC/HAP	2.0 mg CNC/HAP
0	0.0967	1.0632	0.9182	1.1115	0.6283
0.5	17.6738	13.8707	15.9994	17.6166	18.5231
1.0	21.2737	20.2976	20.7340	21.9376	21.7180
1.5	26.9157	25.7624	24.9005	28.0109	28.2192
2.0	27.8327	27.3286	25.4547	28.7296	29.2059
2.5	27.9362	28.2917	26.2973	29.4054	29.1674
3.0	29.6743	27.6650	26.9594	30.3706	29.9359
3.5	30.7904	27.5234	27.2901	30.7164	30.8040
4.0	31.7322	27.8455	28.9943	31.0219	30.4892
4.5	32.4696	28.3233	29.6764	32.5285	32.0658
5.0	33.4937	29.9096	30.1818	33.2360	32.1888
5.5	33.2835	31.1710	30.0912	34.2622	33.2468
6.0	35.8821	32.8670	29.8924	33.7782	32.1218

Table S2: Percentage drug release data in pH ≈ 6.2 from second experiment

Time/hrs	HAP Only	0.5 mg CNC/HAP	1.0 mg CNC/HAP	1.5 mg CNC/HAP	2.0 mg CNC/HAP
0	0.0942	1.1357	1.3290	1.2807	1.0391
0.5	17.2357	13.8008	15.8470	17.0969	18.5624
1.0	19.9699	18.5499	19.6795	20.7849	23.6411
1.5	25.1112	21.7660	24.5039	24.1397	29.6135
2.0	26.1844	24.3570	25.0907	23.8946	31.8599
2.5	27.3547	25.7103	25.8368	24.7926	25.9513
3.0	26.2279	26.0354	25.8486	25.1462	26.7040
3.5	27.4269	26.5597	26.2575	25.2227	33.2132
4.0	28.7187	29.3440	27.7344	27.8360	33.8856
4.5	28.6414	26.8101	29.0815	29.4294	34.1062
5.0	37.7620	30.4500	30.6805	31.2632	35.5521
5.5	34.1003	32.2187	33.4807	33.8439	37.2443
6.0	34.8250	34.0674	34.7697	36.5157	41.3002

Table S3: Percentage drug release data in pH ≈ 6.2 from third experiment

Time/hrs	HAP Only	0.5 mg CNC/HAP	1.0 mg CNC/HAP	1.5 mg CNC/HAP	2.0 mg CNC/HAP
0	0.0992	0.9907	0.4282	0.9861	0.2227
0.5	17.6391	13.9406	16.4596	17.9101	18.4571
1.0	21.7708	22.0453	19.4365	23.2775	20.3829
1.5	28.6437	29.7588	25.5956	31.5938	26.7559
2.0	28.6773	30.3002	25.9546	33.3258	27.4942
2.5	28.2216	30.8731	27.6470	32.8056	29.1674
3.0	33.3181	29.2946	28.2346	35.2647	29.9359
3.5	34.1827	28.4871	28.6254	35.5933	28.4128
4.0	34.5750	26.3470	30.2782	34.4751	27.1252
4.5	36.5330	29.8365	31.1713	35.7251	29.6918
5.0	29.2815	29.3692	29.7407	34.9508	28.6629
5.5	32.6347	31.0243	26.7611	34.2548	29.6009
6.0	35.3792	31.6666	25.0151	31.0407	23.0040

Table S4: Average percentage drug release data in pH ≈ 6.2 from three experiments (Mean±SD)

Time/hrs	HAP Only	0.5 mg CNC/HAP	1.0 mg CNC/HAP	1.5 mg CNC/HAP	2.0 mg CNC/HAP
0	0.0967±0.03	1.0632±0.07	0.8918±0.45	1.1261±0.15	0.6300±0.41
0.5	17.5162±0.24	13.8707±0.06	16.102±0.31	17.5412±0.41	18.5142±0.05
1.0	21.0048±0.93	20.2976±1.74	19.950±0.68	22.0±1.24	21.914±1.63
1.5	26.8902±1.76	25.7624±3.99	25.0±0.55	27.9148±3.72	28.1962±1.42
2.0	27.5648±1.26	27.3286±2.97	25.50±0.43	28.65±4.71	29.52±2.19
2.5	27.8375±0.44	28.2917±2.58	26.5937±0.94	29.0012±4.02	28.0954±1.85
3.0	29.7401±3.54	27.665±1.62	27.0142±1.19	30.2605±5.06	28.8586±1.86
3.5	30.80±3.37	27.5234±0.96	27.391±1.18	30.5108±5.18	30.81±2.40
4.0	31.6753±2.92	27.8455±1.49	29.002±1.27	31.111±3.32	30.50±3.38
4.5	32.548±3.94	28.3233±1.51	29.9764±1.07	32.561±3.14	31.9546±2.20
5.0	33.5124±4.24	29.9096±0.54	30.201±0.47	33.15±1.84	32.1346±3.44
5.5	33.3395±0.73	31.4713±0.65	30.111±3.35	34.1203±0.23	33.364±3.82
6.0	35.3621±0.52	32.867±1.20	29.8924±4.87	33.7782±2.73	32.142±5.14

Table S5: Percentage drug release data in pH ≈ 7.4 from first experiment

Time/hrs	HAP Only	0.5 mg CNC/HAP	1.0 mg CNC/HAP	1.5 mg CNC/HAP	2.0 mg CNC/HAP
0	1.4498	0.7974	0.7249	0.7491	1.0874
0.5	14.2721	6.2120	7.6506	6.5025	5.3860
1.0	16.8314	9.7571	10.8649	9.2944	7.5083
1.5	21.2684	13.0604	14.3132	11.9598	10.3933
2.0	22.6711	14.8367	15.1700	14.0543	12.4022
2.5	22.7452	16.7831	15.8422	15.2042	13.8132
3.0	24.0614	17.8355	16.9808	16.0393	14.9291
3.5	25.2010	17.9250	17.0635	16.5198	15.5944
4.0	25.3360	17.3388	17.2254	17.5133	16.4460
4.5	25.5886	17.2880	18.0588	17.5092	16.4557
5.0	26.7411	17.5155	18.3099	18.6690	17.2727
5.5	26.6953	17.2393	18.0235	19.9340	18.6915
6.0	27.9523	18.8713	16.4058	23.3230	19.6032

Table S6: Percentage drug release data in pH ≈ 7.4 from second experiment

Time/hrs	HAP Only	0.5 mg CNC/HAP	1.0 mg CNC/HAP	1.5 mg CNC/HAP	2.0 mg CNC/HAP
0	1.7398	0.6283	0.7008	0.6041	1.4740
0.5	17.1940	8.9758	10.1957	7.5587	7.8042
1.0	21.3579	7.7840	11.5870	11.7406	9.4318
1.5	21.4210	12.9535	13.1094	12.2558	11.5145
2.0	23.7658	16.8080	16.2398	12.9207	14.0175
2.5	27.6047	17.5119	17.0902	13.9816	14.9708
3.0	22.9254	18.9470	14.9318	14.7743	16.5453
3.5	24.4968	19.1309	15.8532	17.5127	15.8200
4.0	26.2678	18.1916	17.8058	18.1269	17.0076
4.5	29.5970	16.6732	18.4543	17.6818	15.9217
5.0	30.2565	14.8967	19.1324	18.7045	18.7731
5.5	28.7515	18.6554	18.0770	19.5035	18.8518
6.0	30.3352	19.2618	17.4067	23.7197	19.7630

Table S7: Percentage drug release data in pH ≈ 7.4 from third experiment

Time/hrs	HAP Only	0.5 mg CNC/HAP	1.0 mg CNC/HAP	1.5 mg CNC/HAP	2.0 mg CNC/HAP
0	1.1604	0.9746	0.7496	0.8857	0.7089
0.5	11.2359	3.1482	5.1337	5.4388	3.8298
1.0	13.2047	11.2619	9.6481	6.9886	6.2229
1.5	21.2442	12.9711	15.4624	11.7994	9.3282
2.0	21.5371	12.9389	14.1722	14.9740	11.3083
2.5	18.5511	15.2092	15.0676	16.1862	13.2160
3.0	24.8812	17.2175	19.3934	17.6214	13.5256
3.5	25.6745	16.9501	18.3503	15.4555	16.1026
4.0	23.3962	16.6726	16.6168	16.3648	16.0344
4.5	24.6534	17.0748	17.8199	17.4770	17.1526
5.0	23.4440	20.1328	16.5577	18.7325	15.8962
5.5	24.0292	16.3053	18.0525	20.5625	18.0077
6.0	25.5745	18.8399	15.7587	22.9455	19.4338

Table S8: Average percentage drug release data in pH ≈ 7.4 from three experiments (Mean±SD)

Time/hrs	HAP Only	0.5 mg CNC/HAP	1.0 mg CNC/HAP	1.5 mg CNC/HAP	2.0 mg CNC/HAP
0	1.45±0.28	0.8001±0.17	0.725±0.02	0.7463±0.14	1.0901±0.38
0.5	14.24±2.97	6.112±2.91	7.66±2.53	6.50±1.05	5.6733±2.00
1.0	17.1313±2.08	9.601±1.74	10.7±0.97	9.3412±2.37	7.721±1.61
1.5	21.3112±0.09	12.995±0.05	14.295±1.17	12.005±0.23	10.412±1.09
2.0	22.658±1.11	14.8612±1.93	15.194±1.03	13.983±1.02	12.576±1.36
2.5	22.967±2.53	16.5014±1.17	16.0±1.02	15.124±1.10	14.0±0.89
3.0	23.956±0.98	18.0±0.87	17.102±2.23	16.145±1.42	15.0±1.51
3.5	25.1241±0.59	18.002±1.09	17.089±1.24	16.496±1.02	15.839±0.25
4.0	25.0±1.46	17.401±0.76	17.216±0.59	17.335±0.89	16.496±0.48
4.5	26.613±2.62	17.012±0.31	18.111±0.32	17.556±0.11	16.51±0.61
5.0	26.8138±2.40	17.515±2.61	18.0±1.31	18.702±0.03	17.314±1.43
5.5	26.492±2.36	17.40±1.18	18.051±0.02	20.0±0.53	18.517±0.44
6.0	27.954±2.38	18.991±0.23	16.5237±0.83	23.3294±0.38	19.60±0.16

Table S9: Tukey test showing pairwise comparison of samples across groups.

Pairwise comparison	P-value
HAP Only (pH ≈ 6.2) – HAP Only (pH ≈ 7.4)	0.7581
0.5 mg CNC/HAP (pH ≈ 6.2) - 0.5 mg CNC/HAP (pH ≈ 7.4)	0.0191
1.0 mg CNC/HAP (pH ≈ 6.2) – 1.0 mg CNC/HAP (pH ≈ 7.4)	0.0316
1.5 mg CNC/HAP (pH ≈ 6.2) - 1.5 mg CNC/HAP (pH ≈ 7.4)	0.0014
2.0 mg CNC/HAP (pH ≈ 6.2) – 2.0 mg CNC/HAP (pH ≈ 7.4)	0.0004

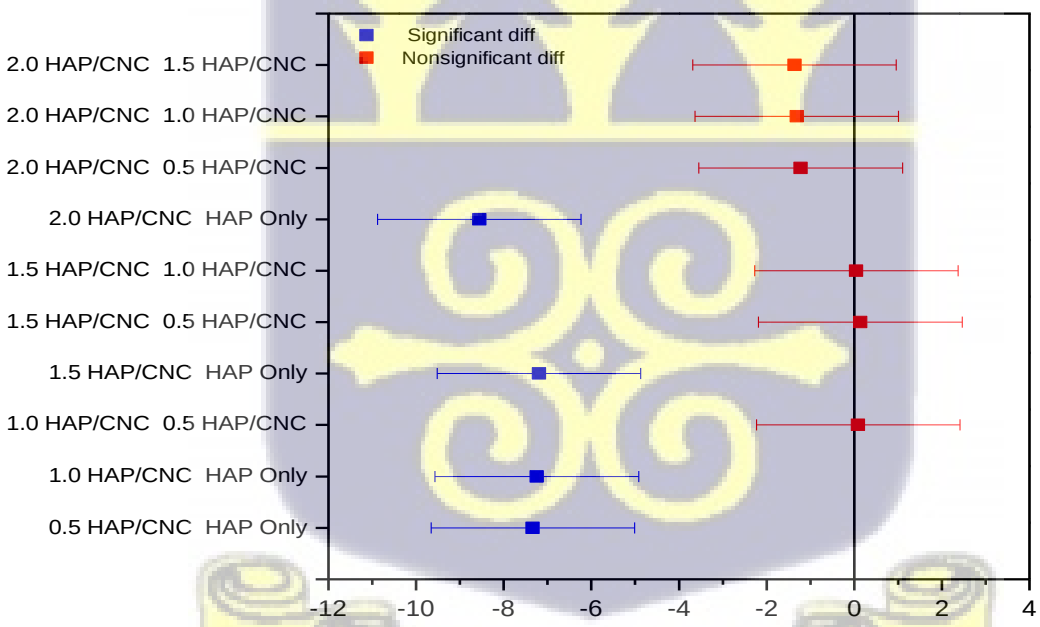

Figure S1: Tukey post hoc test showing difference between composites and control in pH≈ 7.4

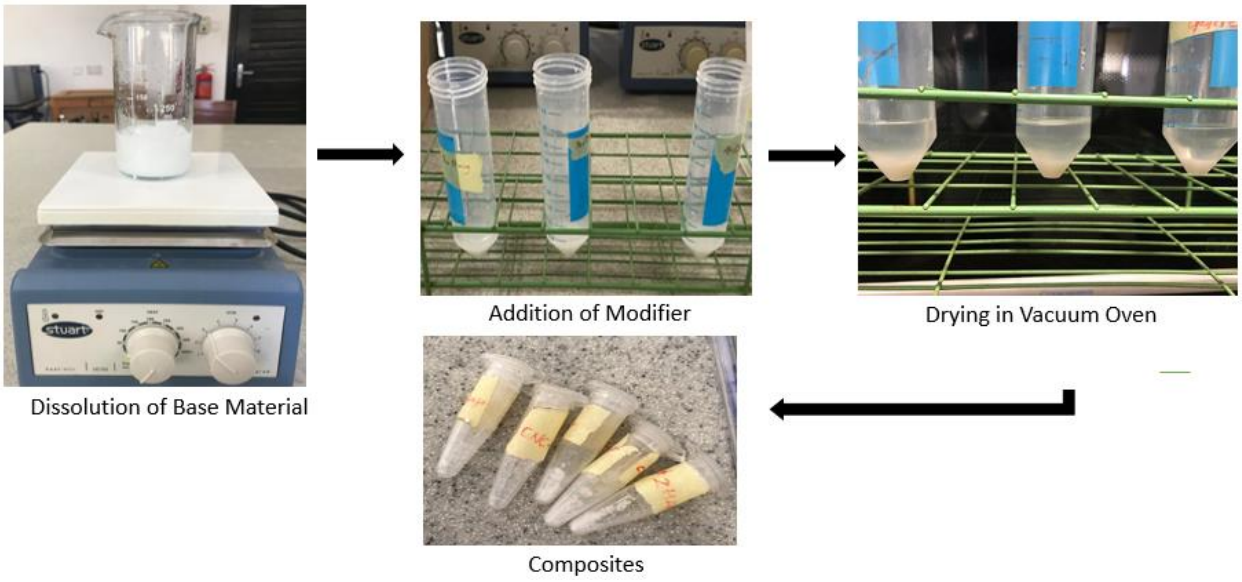

Figure S2: Synthesis of composites

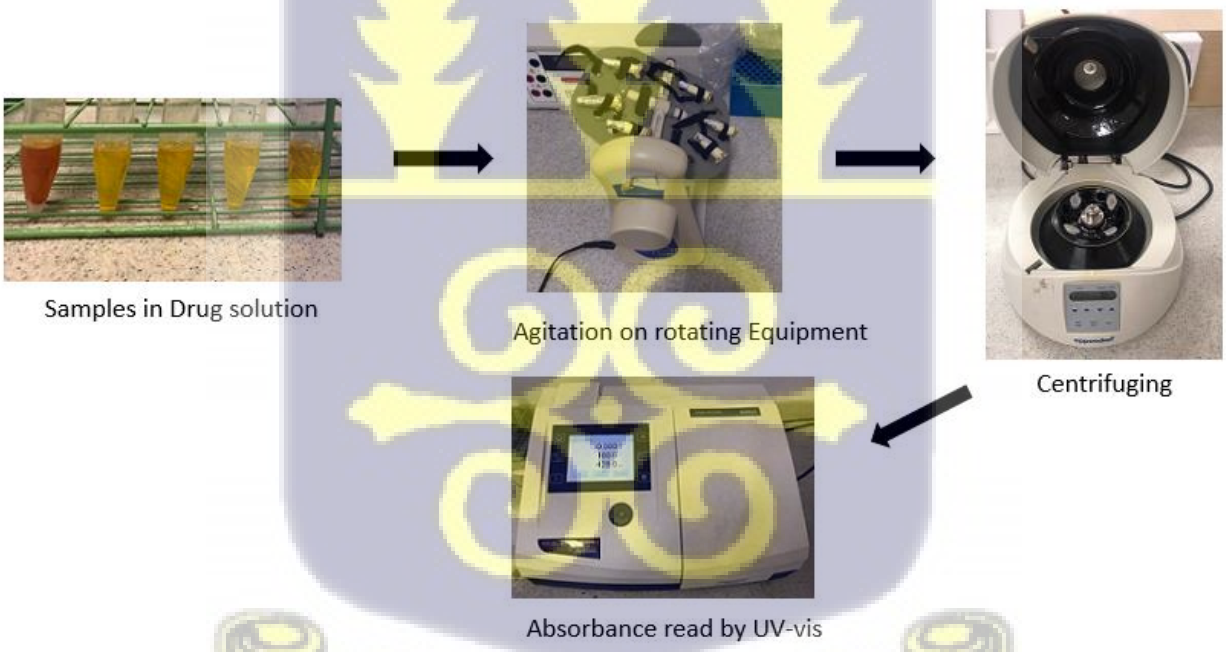

Figure S3: Drug upload experiment

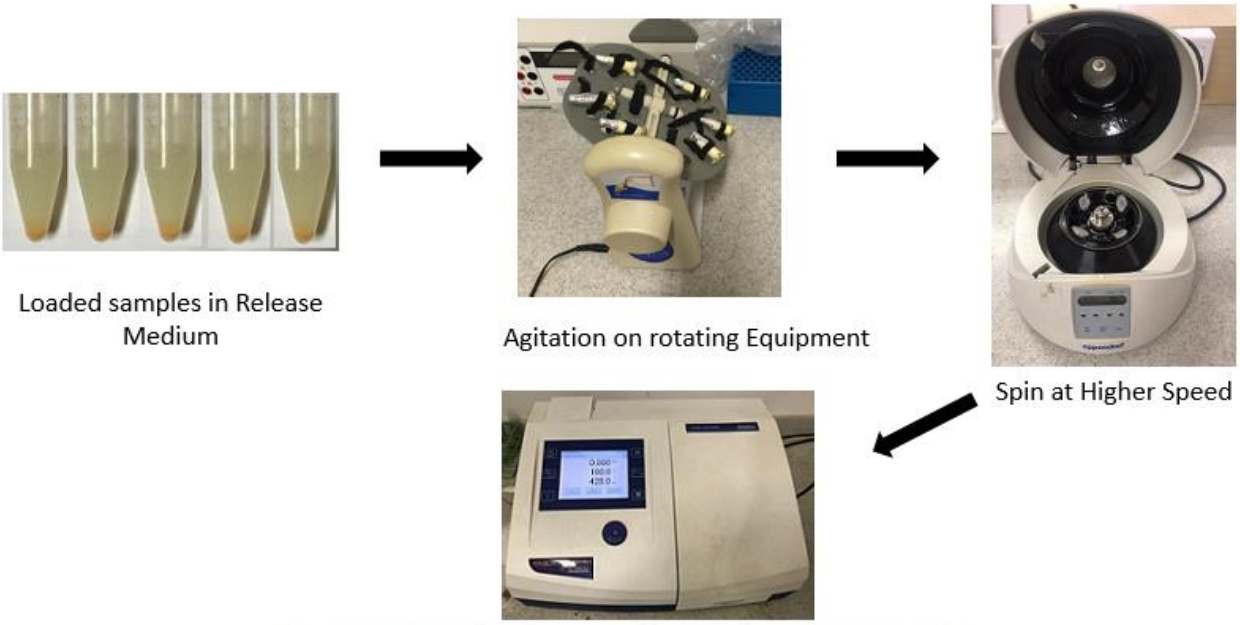

Figure S4: Drug release experiment